https://doi.org/10.5194/se-2019-153
Preprint. Discussion started: 28 October 2019

Solid Earth Discussions
Open Access

Diagenetic evolution of fault zones in Urgonian microporous carbonates, impact on reservoir properties (Provence – SE France).

Irène Aubert [a], Philippe Léonide [a], Juliette Lamarche [a], Roland Salardon [a]

[a] Aix-Marseille Université, CNRS, IRD, Cerege, Um 34, 3 Place Victor Hugo (Case 67), 13331 Marseille Cedex 03, France

Abstract

Microporous carbonate rocks form important reservoirs with high a permeability variability depending of sedimentary, structural and diagenetic factors. Carbonates are very sensitive to fluids-rock interactions that trigger to secondary processes like cementation and dissolution leading to reservoir properties modifications. As they can act as drains or barriers, fault zones influence the fluid flows in the upper part of Earth crust and increase the fluid-rock interactions. The aim of this study is to identify fault zone impact on fluid flows and reservoir properties during basin geodynamic history. The study focuses on 2 fault zones of the Eastern part of La Fare Anticlinal (SE France) where Urgonian microporous carbonates underwent polyphase tectonics and diagenesis. We took 122 samples along 4 transects cross-cutting two fault zones. Porosity values have been measured on 92 dry plugs. Diagenetic properties of samples have been determined on 92 thin sections using Polarized Light Microscopy, cathodoluminescence, red alizarin, SEM and isotopic measurements ($\delta^{13}C$ and $\delta^{18}O$). Height calcite cement stages and 2 micrite micro-fabrics have been identified. This study highlight that fault zones acted as drain canalizing low temperature fluids at their onset, and induced fault zone cementation with two cementation phases, what has strongly altered and modified local reservoir properties.

I. Introduction

Microporous carbonates form important reservoir (Deville de Periere et al., 2017; Lambert et al., 2006; Sallier, 2005; Volery et al., 2009) with porosities up to 35% (Deville de Periere et al., 2011). However, they have heterogeneous properties depending on sedimentary, structural and diagenetic factors, inducing high variability of the reservoir permeability (Bruna et al., 2015; Deville de Periere et al., 2011, 2017; Eltom et al., 2018; Florida et al., 2009; Hollis et al., 2010). Fault zones in carbonates play an important role on reservoir properties (Agosta et al., 2010, 2012; Caine et al., 1996; Delle Piane et al., 2016; Ferraro et al., 2019; Knipe, 1993; Laubach et al., 2010; Rossetti et al., 2011; Sinisi et al., 2016; Solum et al., 2010; Solum and Huisman, 2016; Tondi, 2007; Wu et al., 2019). Fault zones are complex structures composed of the host rock (undeformed protolith), the damage zone and the fault core (Caine et al., 1996; Chester and Logan, 1986, 1987; Hammond and Evans, 2003). They can act as barriers (Agosta et al., 2010; Tondi, 2007), drains (Agosta et al., 2007, 2008, 2012; Delle Piane et al., 2016;

https://doi.org/10.5194/se-2019-153
Preprint. Discussion started: 28 October 2019

Evans et al., 1997; Molli et al., 2010; Reches and Dewers, 2005; Sinisi et al., 2016; Solum and Huisman, 2016), or mixed zones (Matonti et al., 2012) depending of their architecture and diagenetic evolution. Because of their hydraulic properties, fault zones, including fracture network and fault core, influence the fluid flows in the upper part of Earth crust (Bense et al., 2013; Evans et al., 1997; Knipe, 1993; Sibson, 1994; Zhang et al., 2008) and increase the fluids-rock interaction. Carbonates are very sensitive to these fluids-rock interactions that lead to secondary processes like cementation and dissolution (Deville de Periere et al., 2017; Fournier and Borgomano, 2009; Lambert et al., 2006). Fault zones related diagenetic processes locally modifying the initial rock properties (mineralogy and porosity) and therefore their reservoir properties (Hodson et al., 2016; Knipe, 1993; Knipe et al., 1998; Laubach et al., 2010; Woodcock et al., 2007). In case of poly-phase fault zones, duplications of fluid pathways lead to even more complex diagenetic modifications. The initial vertical and lateral compartmentalization of microporous limestones is, therefore, accentuated by these diagenetic modifications. Hence, understanding the impact of fault-related diagenesis on reservoir properties is crucial for a better exploration and production in carbonates. Urgonian microporous carbonates of Provence, present facies and reservoir properties analogue to Middle East microporous carbonate reservoirs (Thamama, Kharaib and Shuaiba formations ;Borgomano et al. 2002, 2013; Sallier 2005; Fournier et al. 2011; Leonide et al. 2012; Léonide et al. 2014). To have a better comprehension of diagenetic modifications linked to fault zones on these rocks, the aim of this paper is (i) to determine the diagenetic evolution of polyphase fault zones, (ii) to identify their impact on reservoir properties and (iii) to link the fault evolution with the fluid flow and geodynamic history of the basin. To this purpose, we targeted Urgonian microporous carbonates of Provence, which are outcrop analogue for the above mentioned underground reservoirs. (Borgomano et al., 2002, 2013; Fournier et al., 2011; Leonide et al., 2012; Léonide et al., 2014; Sallier, 2005).

II. Geological context

We studied two faults affecting Urgonian microporous Valanginian to early Aptian carbonates of the South-East basin (Provence-SE France). They were deposited on the southern margin of the Vocontian basin (Léonide et al., 2014; Masse and Fenerci Masse, 2011). These so-called “Urgonian” platform carbonates (Masse, 1976) reach their larger extension during the late Hauterivian–Early Aptian (Masse and Fenerci-Masse, 2006). From Albian to Cenomanian, the regional Durancian uplift triggered exhumation and erosion of early cretaceous carbonates, bauxitic deposits (Guyonnet-Benaize et al., 2010; Lavenu et al., 2013; Léonide et al., 2014; Masse and Philip, 1976; Masse, 1976) and E-W-trending normal faults (Guyonnet-Benaize et al., 2010; Masse and Philip, 1976). During the Late-Cretaceous, the return to platform environment led to a transgressive rudist platform deposition (Philip, 1970). From the Late cretaceous to Eocene, the convergence of Iberia plate toward Eurasia plate (e.g. Bestani 2015

https://doi.org/10.5194/se-2019-153
Preprint. Discussion started: 28 October 2019

and cited references) led to a regional N-S shortening (e.g. Molliex et al. 2011 and cited references) so-called "Pyrénéo-Provençal" shortening. This compression gave rise to E-W North-verging thrust faults and ramp folds (e.g. Bestani et al. 2016 and cited references). From Oligocene to Miocene, the area underwent extension associated to Liguro-Provençal basin opening (e.g. Demory et al. 2011). During Mio-Pliocene times, the Alpine shortening dimly impacted the studied area (Besson, 2005; Bestani, 2015) reactivating "Pyrénéo-Provençal" structures (Champion et al., 2000; Molliex et al., 2011).

We studied two faults included in a kilometric-scale fault pattern on the E-W-trending La Fare anticline near Marseille (Fig.1A). The southern limb of this anticlinal is dipping of 25° S and is constituted by Upper Hauterivian, Lower Barremian and Santonian rocks (Fig.1B). The Upper Barremian carbonates are composed, from bottom to top, of (1) a 120m thick calcarenite unit with cross-beddings, (2) a 40m thick massive coral-rich calcarenite unit and (3) a 10m thick calcarenite unit (Masse, 1976; Matonti et al., 2012; Roche, 2008). Unconformable Santonian rocks are made of coarse rudist limestones (Fig. 2A).

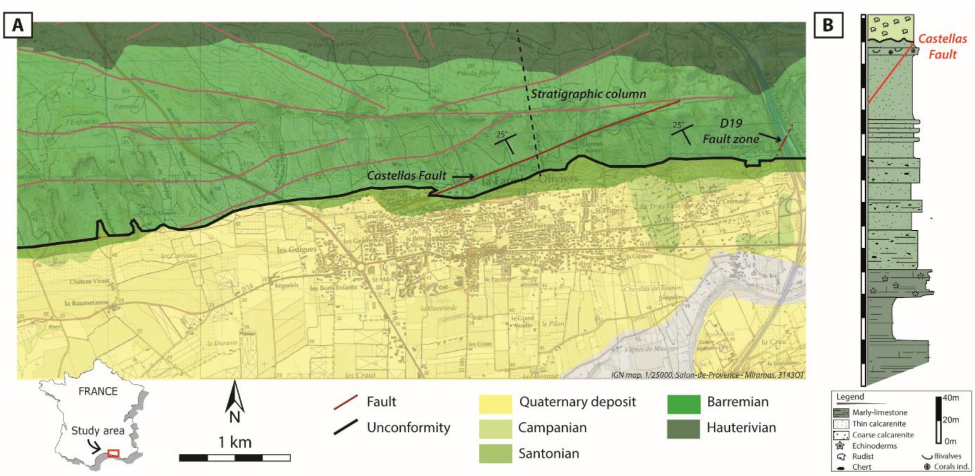

Figure 1 : Geological context of the study area. A: Simplified structural map with the location of the Castellas fault and the stratigraphic column (black dashed line); B: Stratigraphic column of exposed cretaceous carbonates (modified from Roche, 2008)

III. Data Base

We performed 4 transects (T1 to T4) across the Castellas fault and the D19 fault (Fig. 2). The Castellas fault zone is a one kilometer-long strike-slip fault, N060 to 070-trending and 40° to 80°N-dipping with a metric apparent throw (Fig. 2A, 2B).

https://doi.org/10.5194/se-2019-153
Preprint. Discussion started: 28 October 2019

Solid Earth
Discussions

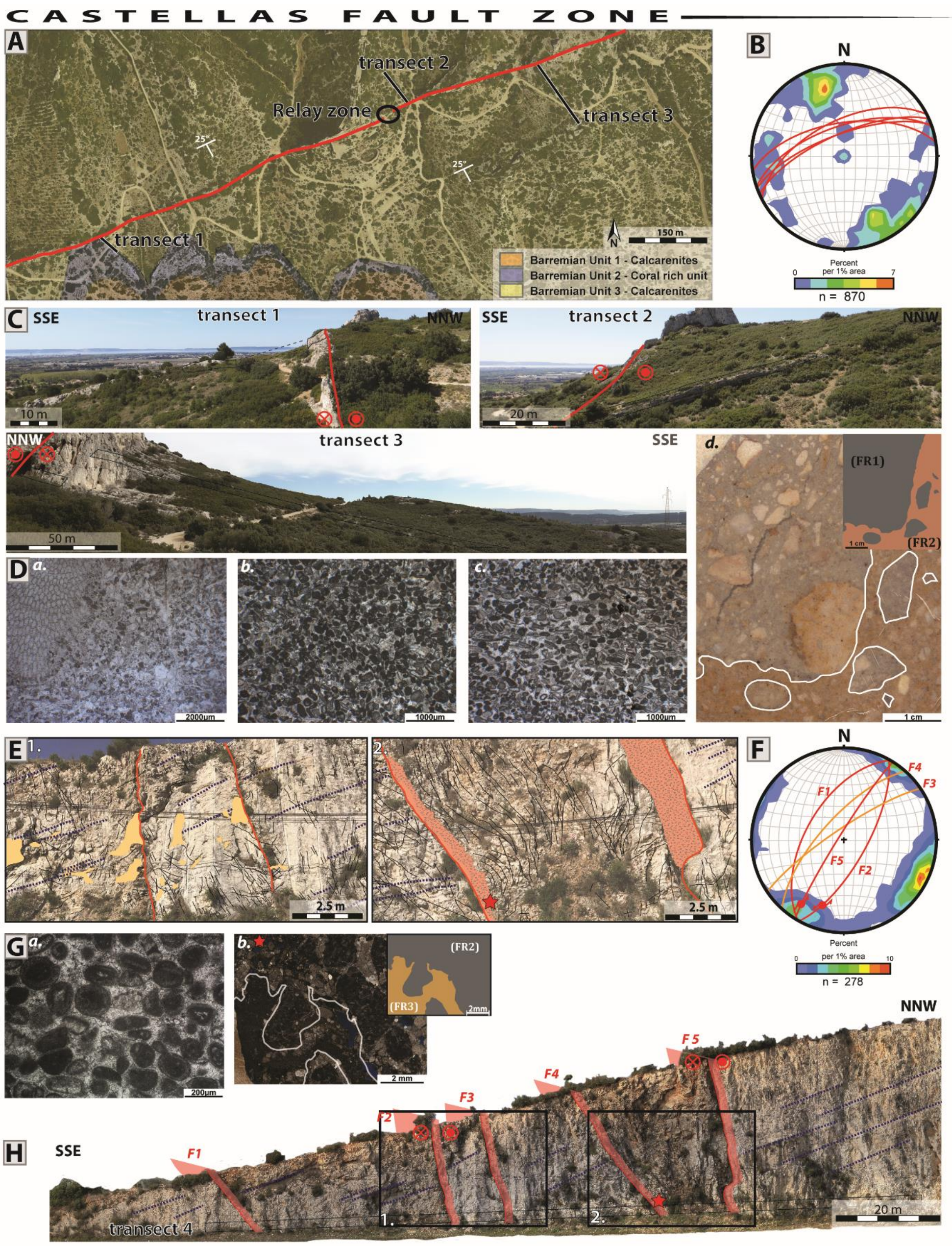

Figure 2 : A: Castellas fault map on aerial photo with localization of the studied transects and the relay zone; B: stereographic projections of poles to fractures (density contoured) and faults (red points) (Allmendinger et al., 2013; Cardozo and Allmendinger, 2013)*; C: Photos of transects; D: Carbonate host rock facies (a) transect 1 coral rich unit, (b) transect 2 calcarenites, (c) transect 3 calcarenites and (d) fault rocks 1 and 2; E: pictures of D19 outcrop F: stereographic projections of poles to fractures (density contoured), set one faults (orange) and set 2 faults*

https://doi.org/10.5194/se-2019-153
Preprint. Discussion started: 28 October 2019

(red) G: Host rock facies (a) and of fault rocks (b); H: D19 outcrop including the five faults F1 to F5.

The fault zone has a heterogeneous anastomosed architecture, made of duplex and horse structures. (Fig. 2A, 2C; Aubert et al. (2019b). Transect T1 is located along the coral rich unit 2. This bed is essentially composed of pelloidal grains and bioclasts (corals, bivalves and stromatoporidae; Fig. 2D a). Transects T2 and T3 are located in unit 3, made of fine calcarenites with pelloidal grains and a rich fauna (foraminifera, bivalves, ostracods and echinoderm; Fig. 2Db, c). The second fault zone “D19” is composed of 5 sub-fault zones restricted in a 50m-long interval (Fig. 2E, H). Sub-faults are made of 2 sets. The set one, constituted of F3 and F4, is N040 to N055-trending and 60-80°NW-dipping (orange on Fig. 2F). The set two is N030-trending, dipping 80°E, with strike-slip slickensides pitch 20 to 28°SW (F1, F2, F5, red on Fig. 2F). The 5 sub-fault zones show an asymmetric architecture (Aubert et al., 2019a). Transect 4 has been realized along the D19 outcrop (Fig. 3) exhibiting Barremian outer platform bioclastic calcarenite with current ripples. The grains are mainly peloids with minor amount of bioclasts (solidary corals, bryozoan, bivalves and some rare miliolids; Fig. 2G, a). The structure of both polyphase fault zones results from three tectonic events:

- the Durancian uplift dated as mid-Cretoceous leading to extension and to normal *en echelon* normal faults. The Castellas fault is one of them and bear early dip-slip normal striations (Matonti et al., 2012),
- the Early Pyrenean compression with N000° to N170°-trending σ_H (see cited references in Espurt et al. 2012). This event reactivates the Castellas fault as sinistral (Matonti et al., 2012) and leads to the neo-formed strike-slip faults of the D19 outcrop (Aubert et al., 2019a).
- the Pyrenean to Alpine folding, triggering the 25°S tilting of the strata and fault zones. Faults of the D19 outcrop were reactivated while the Castellas fault tilting led to an apparent reverse throw (Aubert et al., 2019a).

These tectonic events impacted the fault zone and fault core structure. Both faults have different fault cores (Table 1) made of 3 fault rock types in Castellas (Matonti et al., 2012) and D19 fault zones (see Aubert et al. 2019a).

Table 1: structural properties of the fault zones

Faut zones	Faille	Direction	Dip	Dip direction	pitch striation	Fault core thickness	Fault Rocks		
							FR1	FR2	FR3
Castellas	Castellas	060 - 070	40 to 80	N	14W -	0 to 4m	sparsely present	majoritarely present	/
D19	F1	030	56	W		20	/	<10 cm	/
	F2	029	70	E	28 S	10 to 15	/	?	non constant thickness
	F3	056	80	N		0 to 15	/	?	?
	F4	042	70	W		20	/	in the clasts of FR3	non constant thickness
	F5	032	85	N	20 SW	50 to100	/	/	non constant thickness

https://doi.org/10.5194/se-2019-153
Preprint. Discussion started: 28 October 2019

Solid Earth Discussions

Fault rock 1 (FR1) results from the normal activation of the Castellas fault during Durancian uplift. It is a cohesive breccia composed of sub-rounded to rounded clasts from the nearby damage zone and in <30% of grey matrix (Fig. 2Dd). Fault rock 2 (FR2), is linked to the sinistral reactivation of the Castellas fault and the onset of D19 fault zone during the Pyrenean shortening. FR2 present two morphologies depending on the fault zones. Within Castellas fault, FR2 is an un-cohesive breccia with an orange/oxided matrix with angular to sub-rounded clasts from the damage zone and from FR1 (Fig. 2Dd). In the D19 fault zone, FR2 is a cohesive breccia with rounded clasts of the damage zone and a white cemented matrix (Fig. 2Gb). Fault rock 3 (FR3) is formed by the reactivation of D19 fault zone. It is composed of angular to sub-angular clast from FR2 and from the nearby damage zone in an orange/oxided matrix (<20%) (Fig. 2Gb).

II. Methods

The data set comprises 122 samples, 62 from Castellas and 60 from D19 outcrops, collected along the 4 transects. Porosity values have been measured on 92 dry plugs with a Micromeritics AccuPyc 1330 helium pycnometer. Characterization of microfacies and petrography have been determined on 92 thin sections. The impregnation with a blue-epoxy resin allows to decipher the different pore types. Thin sections were coloured with Alizarin red S and potassium ferricyanide to distinguish carbonate minerals (calcite and dolomite). The thin sections have been analyzed using cathodoluminescence to quantify how the diagenesis and the fault zone setup affected the initial rock properties. The paragenetic sequence has been defined based on superposition and overlap principles observed on thin sections using a Technosyn Cold Cathode Luminescence Model 8200 Mk II coupled to an Olympus_ BH2 microscope and to a Zeiss_ MR C5. Micrite micro-fabric and major element composition of 2 samples from the fault zone, 2 from the host rock and 1 from the D19 karst infilling were measured using PHILIPS XL30 ESEM with a current set at 20kV on fresh sample surface and on thin sections. To determine stable carbon and oxygen isotopes ($\delta^{13}C$ and $\delta^{18}O$), 207 microsamples (<5 mg) were drilled, 187 of them were micro-drilled from polished thin sections with an 80 µm diameter micro-sampler (Merkantec Micromill) at the VU University (Amsterdam, The Netherlands). We sampled 59 bulk rocks, 74 sparitic cements, 38 fault rocks and 23 micrite. Carbon and oxygen values were acquired with the Gasbench II and the Finnigan DeltaPlus IRMS. We corrected the sample size using the VICS carbonate standard. The international control standard applied was the IAEA-603 (values of +2.46‰ for $\delta^{13}C$ and -2.37‰ for $\delta^{18}O$). Ten whole rock samples were analysed using a Gasbench II connected to a Thermo Fisher Delta V Plus mass spectrometer at

https://doi.org/10.5194/se-2019-153
Preprint. Discussion started: 28 October 2019

the FAU University (Erlangen, Germany). Measurements were calibrated by assigning $\delta^{13}C$ values of +1.95‰ to NBS19 and -47.3‰ to IAEA-CO9 and $\delta^{18}O$ values of -2.20‰ to NBS19.

III. Results

1. Microporosity and porosity

Porosity measurements have been achieved on the 92 samples collected along the 4 transects (T1 to T4). In average, the porosity strongly decreases towards the fault (Fig. 3): from >10% (mean: 15%, SD: 2.68 for Castellas and mean 12.3%, SD: 2.52 for D19) to < 5% in fault zones (mean: 4.8%, SD: 2.07 for Castellas and mean: 3.16%, SD: 2.35 for D19).

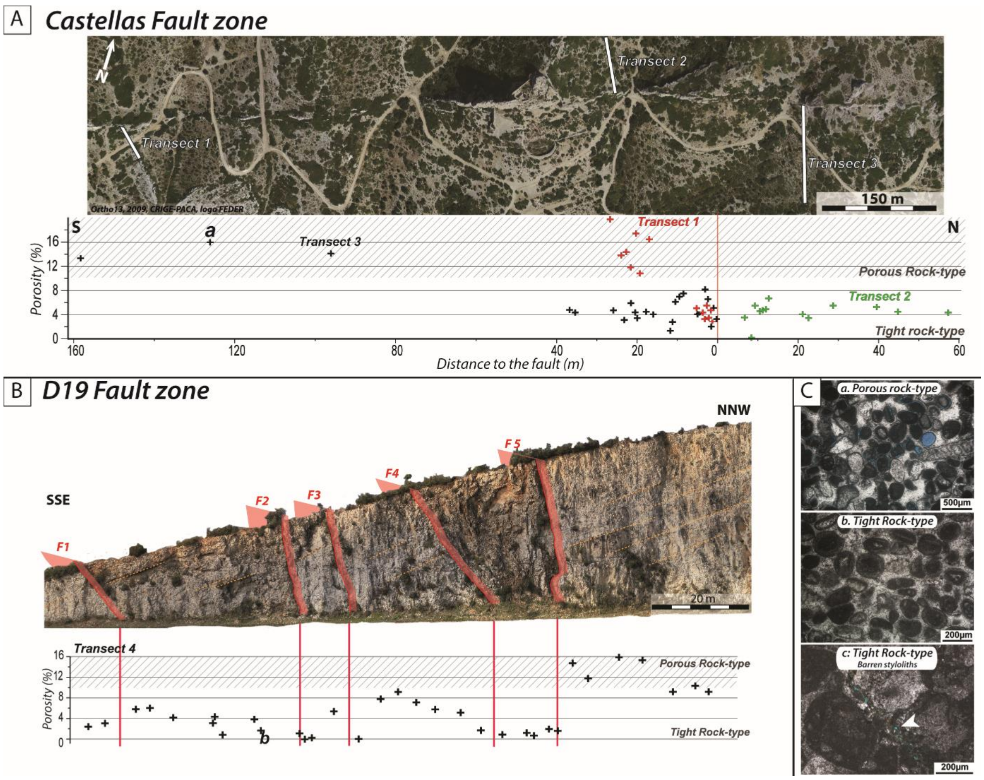

Figure 3: A: Castellas fault zone aerial view (Ortho13, 2009, CRIGE-PACA, logo FEDER) & porosity values measured along transect 1 (Red Cross), transect 2 (green cross) and transect 3 (black cross); B: porosity values measured along D19 fault zone; C: Pore types in the host rock (a) and in the fault zones (b&c).

Some variations occur as follows:

- North of the Castellas fault, along the 60m-long transect T2 the porosity is constantly low < 7% (mean of 4.4%, SD:1.53 ; Fig. 3A),

https://doi.org/10.5194/se-2019-153
Preprint. Discussion started: 28 October 2019

- South of the Castellas fault, the reduced porosity zone is >40m in transect 3 and 30m in transect 1 (Fig. 3A). In a 10m-thick zone from the fault plane, porosity reduction occurs with lower values in T1 (average 4.9%) than in T3 (average 5.6%).
- In the D19 fault zone, the lowest porosity values are in narrow (less than 2m) zones around the faults and in the lens between F4 and F5. Though, this porosity decrease is not homogeneous in fault zone and high values are found north of F1 and F3 (Fig. 3B).

From thin sections impregnated with blue-epoxy resin we distinguished two rock-types: a porous rock-type with $\varphi>10\%$ moldic and microporosity in micritized grains (Fig. 3C a) and a tight rock-type with $\varphi< 5\%$ where the porosity is mostly linked to barren styloliths (Fig. 3C b, c).

2. Diagenetic phases

a. Micrite micro-fabric

Micritized bioclasts, ooids and peloids were observed with SEM on 2 samples from fault zones and 2 samples from the host rock. Two micro-fabrics of micrite is define with specific crystal shape, sorting and contacts according to *Fournier et al.* (2011). Within both fault zones, the micrite is tight with compact subhedral mosaic crystals (MF1; Fig. 4A, 4B). In the host rock, the micrite is loosely packed and partially coalescent with puntic rarely serrate, subhedral to euhedral crystals (MF3; Fig. 4C, D, E). MF1 correlates with low porosity values < 5% while MF3 and is associated to higher porosity > 10%.

https://doi.org/10.5194/se-2019-153
Preprint. Discussion started: 28 October 2019

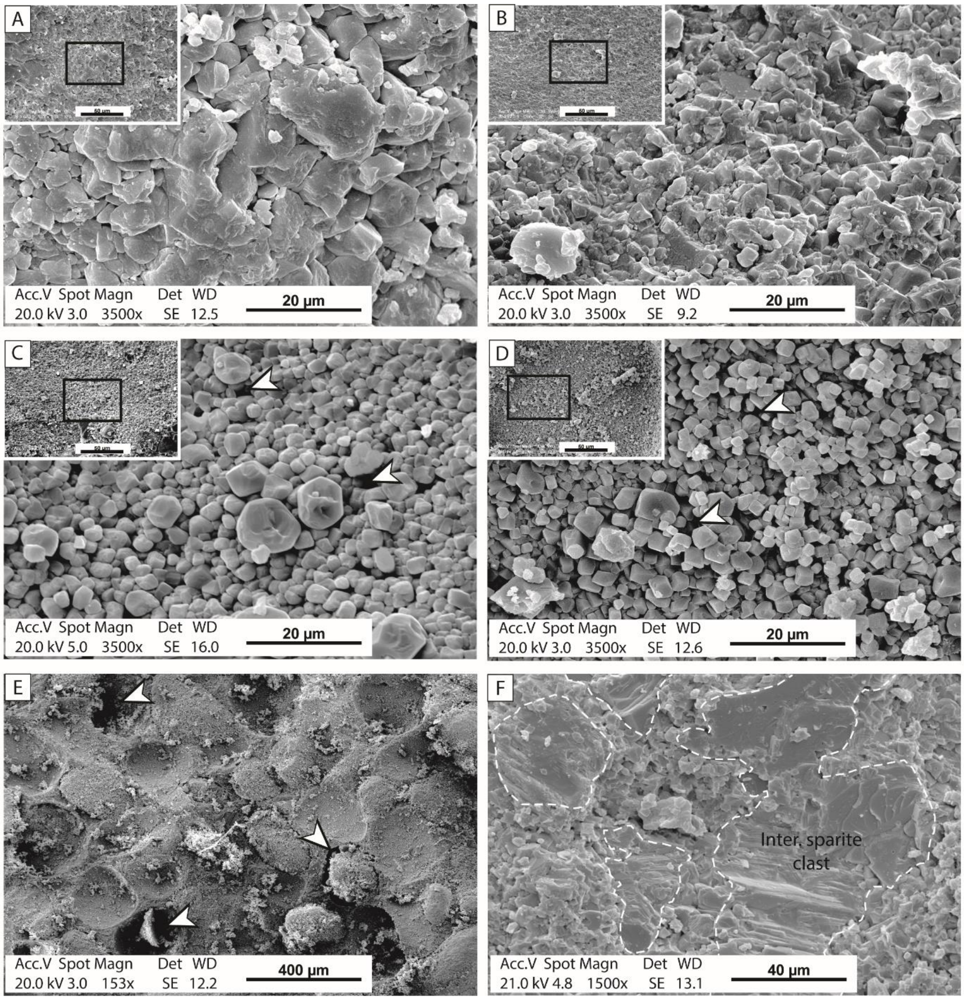

Figure 4 : MEB pictures of micrite micro-fabric and microporosity (white arrow); A. MF1micrite micro-fabric in Castellas fault zone (2.5m to fault plane); B: MF1micrite micro-fabric within D19 fault zones (2m away from F5 fault plane); C: MF3 micrite micro-fabri C: MF3 micrite micro-fabric within Castellas host rock (188m away from the fault plane); D: MF3 micrite micro-fabric within D19 host rock (95m away from F5 fault plane); E: D19 host rock moldic porosity; F. Karst infilling.

b. Diagenetic cements

Height cement stages have been identified (Fig. 5). The red stain links to Alizarin red S coloration shows that all visible cements are calcite. They have variable characteristics (morphology, luminescence, size and location) as described below.

https://doi.org/10.5194/se-2019-153
Preprint. Discussion started: 28 October 2019

The first two cement phases occur in both fault zones. The first cement (C0) is non-luminescent isopachous growing with equal thickness (≈10µm) around grains (Fig. 5A). The second cement (C1) is divided in 2 sub-phases: a non-luminescent calcite C1a with a dog tooth morphology in intergranular spaces and a bright luminescence calcite C1b covering C1a with an average thickness of <10µm and a maximum thickness of ≈100µm (Fig. 5). C1b also fills micro-porosity in micritised grains (Fig. 5B). C1b values strongly increase in Castellas fault zone. Five cements or replacive phases occur largely in the Castellas sector and rarely in the D19 outcrop:

- C2 is a sparitic cement with dull orange luminescence only found in fault core veins (Fig. 5B). SEM measurements show the Si and Al elements in the C2 veins. Most of Si crystals are automorphic.
- C3 is a blocky calcite with non to red dull luminescence in veins, moldic and intergranular pores (Fig. 5B, C, D). This cement also occurs in few veins of D19 sectors but is not restricted to the fault zone.
- Phantoms of planar-e (euhedral) dolomite crystals (Sibley and Gregg, 1987) with a maximum size of 500µm affect the matrix of FR1 (Fig. 5E). They are vestiges of a dolomitization phase. They have a cloudy appearance caused by solid micritic inclusion in the crystal and can be considered as replacive dolomite (RD; Machel, 2004). Within the FR1 matrix, an important concentration of angular grains of quartz with a maximum size of 300µm is noticed (Fig. 5F).
- A blocky calcite C4 (referred to as S2 in Aubert et al. (2019a)) is mainly present in veins of the D19 outcrop, intergranular & moldic pores and in FRA matrix (Fig. 5G, 5H). This cement shows zonation of bright luminescent and non-luminescent bands and can be sub-divided in 2 phases: C4a which is sparitic, non-luminescent with some highly luminescent band and C4b which is sparitic, bright luminescent with some non-luminescent bands. C4a occurs in lesser proportion in some veins along transect T2 and T3 of the Castellas fault.
- A sparitic cement C5, with a red dull luminescence replaces the RD phase (Fig. 5F).

https://doi.org/10.5194/se-2019-153
Preprint. Discussion started: 28 October 2019

Solid Earth
Discussions
Open Access
EGU

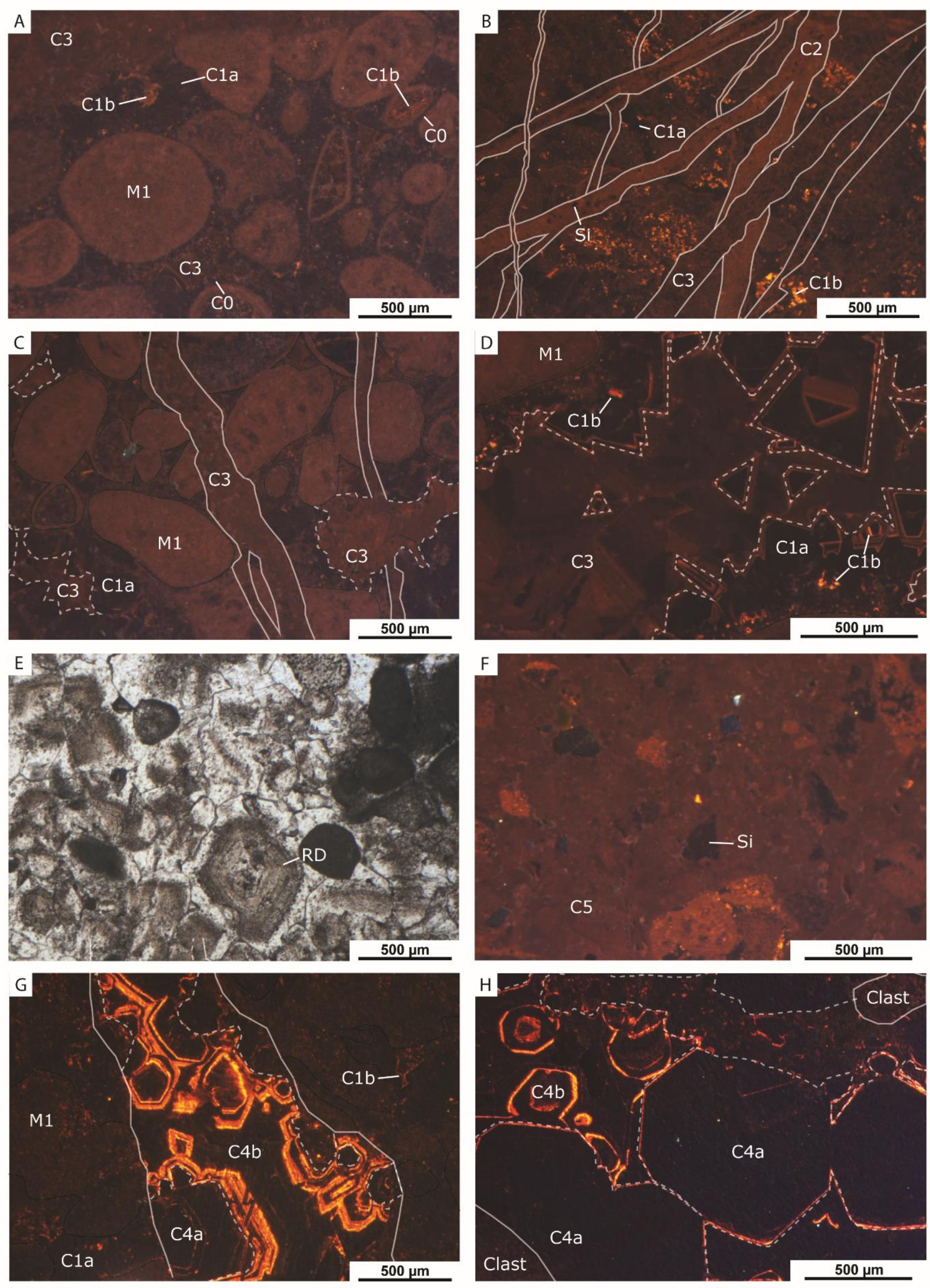

236 *Figure 5 : Thin-sections under cathodoluminescence; A: Calcarenite in transect 3 with micritized grain (M1), and intergranular space cemented with C1 a&b and C3; B: C2 (with Si) and C3 veins affecting Castellas FR1 clast with micritized grains cemented by C1b; C: C3 vein cement and intergranular space in Castellas fault zone; D: C1 (a & b) and C3 cementing moldic porosity of transect 3 calcarenite; E: FR1 matrix with phantom of cloudy appearance replacive dolomite; F: FR1 matrix de-dolomitized by C5 containing quart grains; G: C4 (a & b) cementing vein of D19 fault zone; H: matrix of D19 FR2 cemented by C4 (a&b).*

https://doi.org/10.5194/se-2019-153
Preprint. Discussion started: 28 October 2019

c. Additional diagenetic features

In addition to cementation phases other diagenetic processes affected both fault zones. Karst infilling occurs in the F2 fault zone of the D19 outcrop. It is composed of well-sorted grains deposited in laminated layers. This formation present a stack of micrite-rich layers and grain-rich layers. In the case of grain-rich layers, grains are intergranular sparitic clasts, remaining from blocky calcite of dissolved grainstones, and oxydes. The laminated layers are affected by veins and styloliths, some of them are deformed due to the clasts fall on sediments. Micritic layers has been observed under SEM, the micrite appeared tight with compact subhedral mosaic crystals (Fig. 4F). We observed oxide filling mainly in the Castellas area in dissolution voids affecting C1a, C1b and C3 cementation phases and in D19 in karstic fill. The proportion of oxides increase close to stylolites.

3. Carbone and Oxygene Isotopes

Isotope measurements were realized on samples withdrawn along transect cross cutting both fault zones. A hundred and eighty-nine measurements of C and O isotopes have been performed on 16 samples and 32 thin sections (Fig. 6A, table 2).

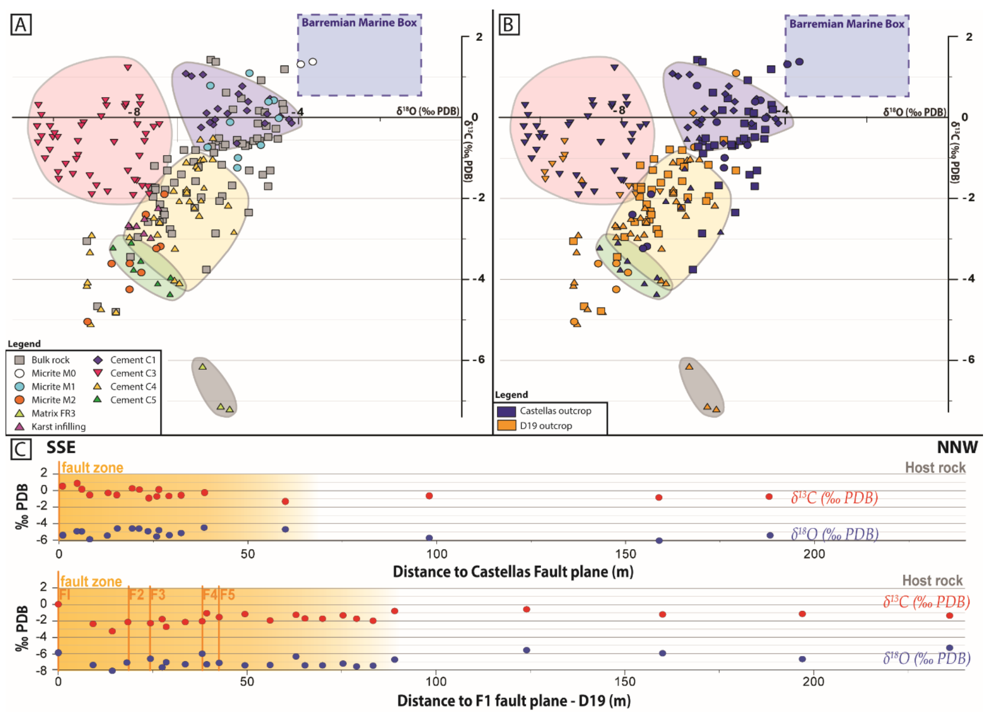

Figure 6 : Isotopic values of δ13C and δ18O measured on bulk rock, cement phases, and micrite. Range values of "Urgonian marine box" from Moss & Tucker (1995) and Godet et al. (2006); A: set of values

https://doi.org/10.5194/se-2019-153
Preprint. Discussion started: 28 October 2019

sorted by the nature of diagenetic phases and B: values sorted by the fault zone; C: lateral evolution of δ13C and δ18O isotopic values in Castellas (top) and in D19 (bottom) fault zones.

Sampling has been done in bulk rock (49), in veins (48), in fault rocks (40) and in intergranular spaces (26) in order to determine the isotopic signature of the diagenetic phases. Isotopic values range from -10.40‰ to -3.65‰ for $\delta^{18}O$ and from -7.2‰ to +1.42‰ for $\delta^{13}C$ (Fig. 6A, 6B, table 2). The bulk rock values range from -8.11‰ to -4.34‰ for $\delta^{18}O$ and from -3.76‰ to +0.47‰ for $\delta^{13}C$ (Fig. 6A, table 2). These values are split in two sets. Set one includes transect 1 & 3 of the Castellas Fault. Bulk values range from -1.4‰ to -1.2‰ for $\delta^{18}O$ and from -6.1‰ to -4.3‰ for $\delta^{13}C$. Set two includes transect 2 (Castellas) and transect 4 (D19). Bulk values range from -8.1‰ to -4.7‰ for $\delta^{18}O$ and from -3.8‰ to -0.5‰ for $\delta^{13}C$ (Fig. 6B, table 2). In the transect 3, the isotopic values only slightly vary along transect, ranging from -6.13‰ to -4.50‰ for $\delta^{18}O$ and from -1.41‰ to +0.47‰ for $\delta^{13}C$ (Fig. 6C, table 2). Contrarily, values vary more along the D19 transect. They range from -8.02‰ to -5.21‰ for $\delta^{18}O$ and from -3.2‰ to +0.54‰ for $\delta^{13}C$ (Fig. 6C, table 2). Indeed, the $\delta^{13}C$ values obviously decrease in the fault vicinity, especially south of F2.

Isotopic values of cements filling veins, intergranular spaces, karst, and fault rock are divided into 5 groups (Fig. 6A, table 2):

- the group of C1 values fluctuates from -6.8‰ to -3.9‰ for $\delta^{18}O$ and from -1.0 to +1.3‰ for $\delta^{13}C$;
- the group of C3 values ranges from -10.40‰ to -6.73‰ for $\delta^{18}O$ and from -2.09 to +1.22‰ for $\delta^{13}C$;
- the group of C4 values in FR1 and FR2 matrix and in karst fill ranges from -9.2‰ to -4.60‰ for $\delta^{18}O$ and from-5.1‰ to -0.74‰ for $\delta^{13}C$ with a positive covariance between $\delta^{18}O$ and $\delta^{13}C$. More precisely, C4 isotopic values ranges from -9.2‰ to -6.1‰ for $\delta^{18}O$ and from -5.1‰ to -1.0‰ for $\delta^{13}C$. FR 2 matrix values (from-6.55 to -7.06‰ for $\delta^{18}O$ and from -1.10 to -2.24‰ for $\delta^{13}C$) present slightly less negative values than karst fill with mean values of -7.83‰ and -2.53‰ respectively for $\delta^{18}O$ and $\delta^{13}C$. (Fig. 6A). In the Castellas fault, 4 isotopic values from two veins are high with means of -6.25 and -4.2‰ for $\delta^{18}O$ -0.64 and -0.09‰ for $\delta^{13}C$ having similar positive covariance than the other C4 values.
- the group of C5 values, sampled in FR1 matrix with a mean of -7.49‰ for $\delta^{18}O$ and -4.01‰ for $\delta^{13}C$ (Fig. 6A).

https://doi.org/10.5194/se-2019-153
Preprint. Discussion started: 28 October 2019

Solid Earth Discussions

- The group of values from FR3 matrix with a mean of -5.98‰ for $\delta^{18}O$ and -6.83‰ for $\delta^{13}C$ (Fig. 6A)

Table 2: Carbon and oxygen isotope values of bulk carbonates for Castellas fault zone and D19 fault zones. B: bulk measurements; M: micrite values; C1, C3, C4, C5: isotopic values of cement C1, C3, C4 and C5; FR: fault rock isotopic values.

Transect	Sample	$\delta^{13}C$ (‰ vs VPDB)	$\delta^{18}C$ (‰ vs VPDB)	Class	Distance to the Fault (m)
Castellas (Transect 1)	201	1,02	-6,62	C1	1,3
Castellas (Transect 1)	201	1,19	-4,34	B	1,3
Castellas (Transect 1)	201	1,31	-3,94	M	1,3
Castellas (Transect 1)	201	1,37	-3,65	M	1,3
Castellas (Transect 1)	213	-2,09	-6,92	C4	22,7
Castellas (Transect 1)	213	-0,68	-4,92	M	22,7
Castellas (Transect 1)	213	-0,68	-5,24	B	22,7
Castellas (Transect 1)	213	-0,58	-5,10	B	22,7
Castellas (Transect 1)	213	-0,18	-6,09	C1	22,7
Castellas (Transect 1)	213	0,03	-4,45	C1	22,7
Castellas (Transect 1)	213	0,09	-4,77	C1	22,7
Castellas (Transect 2)	c3b17	-2,07	-6,38	C4	4,6
Castellas (Transect 2)	c3b17	-0,52	-5,95	B	4,6
Castellas (Transect 2)	c3b7	-0,64	-5,51	B	9,3
Castellas (Transect 2)	c3b26	-3,76	-6,26	B	22,6
Castellas (Transect 2)	c3b26	-2,85	-5,58	C4	22,6
Castellas (Transect 2)	c3b26	-2,35	-5,22	M	57,3
Castellas (Transect 2)	c3b26	-1,70	-4,75	M	57,3
Castellas (Transect 2)	c3b26	-1,31	-4,69	B	57,3
Castellas (Transect 2)	c3b7	-1,76	-6,31	C1	57,3
Castellas (Transect 2)	c3b7	-1,28	-6,46	C1	57,3
Castellas (Transect 3)	327	-3,11	-8,09	C4	0,3
Castellas (Transect 3)	327	-0,24	-7,55	C3	0,3
Castellas (Transect 3)	325	-1,90	-9,06	C3	0,3
Castellas (Transect 3)	325	-1,69	-8,95	C3	0,3
Castellas (Transect 3)	327	-0,18	-7,95	C3	1,0
Castellas (Transect 3)	327	-0,17	-7,41	C3	1,0
Castellas (Transect 3)	327	0,47	-5,40	B	1,0
Castellas (Transect 3)	328	-1,32	-8,18	C3	1,6
Castellas (Transect 3)	328	-0,59	-7,77	C3	1,6
Castellas (Transect 3)	328	-0,42	-7,74	C3	1,6
Castellas (Transect 3)	328	-0,14	-4,17	C4	1,6
Castellas (Transect 3)	328	-0,13	-9,26	C3	1,6
Castellas (Transect 3)	328	-0,05	-4,23	C4	1,6
Castellas (Transect 3)	328	0,02	-8,83	C3	1,6
Castellas (Transect 3)	328	0,10	-5,74	C1	1,6

https://doi.org/10.5194/se-2019-153
Preprint. Discussion started: 28 October 2019

Castellas (Transect 3)	328	0,29	-8,70	C3	1,6
Castellas (Transect 3)	328	0,42	-8,73	C3	1,6
Castellas (Transect 3)	328	0,50	-7,89	C3	1,6
Castellas (Transect 3)	328	1,22	-8,18	C3	1,6
Castellas (Transect 3)	333	-1,84	-8,67	C3	1,6
Castellas (Transect 3)	333	-0,96	-7,89	C3	1,6
Castellas (Transect 3)	329	0,16	-4,95	B	2,4
Castellas (Transect 3)	333	-0,62	-8,52	C3	4,6
Castellas (Transect 3)	333	-0,25	-6,38	C1	4,6
Castellas (Transect 3)	333	-0,12	-6,17	C1	4,6
Castellas (Transect 3)	333	-0,12	-5,67	M	4,6
Castellas (Transect 3)	333	-0,02	-4,48	M	4,6
Castellas (Transect 3)	333	0,42	-4,60	M	4,6
Castellas (Transect 3)	337	0,19	-5,59	B	9,5
Castellas (Transect 3)	302	-0,62	-10,38	C3	11,8
Castellas (Transect 3)	302	-0,53	-4,50	B	11,8
Castellas (Transect 3)	302	-0,49	-10,02	C3	11,8
Castellas (Transect 3)	302	-0,49	-4,74	B	11,8
Castellas (Transect 3)	305	0,33	-4,38	B	16,0
Castellas (Transect 3)	306	0,21	-4,35	B	17,8
Castellas (Transect 3)	307	-0,01	-4,46	B	18,2
Castellas (Transect 3)	308	-1,44	-9,11	C3	20,0
Castellas (Transect 3)	308	-0,57	-4,95	B	20,0
Castellas (Transect 3)	308	-0,23	-10,40	C3	20,0
Castellas (Transect 3)	308	-0,22	-10,08	C3	20,0
Castellas (Transect 3)	309	-1,56	-7,96	C3	20,5
Castellas (Transect 3)	309	-1,55	-8,01	C3	20,5
Castellas (Transect 3)	309	-1,41	-4,87	B	20,5
Castellas (Transect 3)	309	-0,52	-5,01	B	20,5
Castellas (Transect 3)	309	-0,15	-4,82	C1	20,5
Castellas (Transect 3)	312	0,12	-4,81	B	23,2
Castellas (Transect 3)	314	-0,80	-10,09	C3	25,9
Castellas (Transect 3)	314	-0,71	-5,30	B	25,9
Castellas (Transect 3)	314	-0,49	-9,90	C3	25,9
Castellas (Transect 3)	314	-0,47	-10,29	C3	25,9
Castellas (Transect 3)	314	-0,40	-9,97	C3	25,9
Castellas (Transect 3)	314	0,06	-10,30	C3	25,9
Castellas (Transect 3)	316	-1,24	-5,50	B	29,2
Castellas (Transect 3)	316	-1,02	-10,21	C3	29,2
Castellas (Transect 3)	316	-1,00	-5,48	B	29,2
Castellas (Transect 3)	316	-0,22	-4,79	B	29,2
Castellas (Transect 3)	316	-0,18	-9,31	C3	29,2
Castellas (Transect 3)	316	0,30	-10,37	C3	29,2
Castellas (Transect 3)	318	-0,28	-4,53	B	35,4
Castellas (Transect 3)	320	-0,68	-5,79	B	96,1

https://doi.org/10.5194/se-2019-153
Preprint. Discussion started: 28 October 2019

Solid Earth Discussions
Open Access
EGU

Castellas (Transect 3)	322	-0,88	-6,07	B	158,0
Castellas (Transect 3)	323	-0,65	-5,37	B	188,0
Castellas (ZF1)	Z1,1	-0,55	-6,40	C4	0,0
Castellas (ZF1)	Z1,1	-0,52	-6,10	C4	0,0
Castellas (ZF1)	Z1,1	0,17	-5,26	C1	0,0
Castellas (ZF1)	Z1,1	0,39	-5,23	C1	0,0
Castellas (ZF1)	Z1,1	0,46	-4,70	C1	0,0
Castellas (ZF1)	Z1,1	0,78	-6,16	M	0,0
Castellas (ZF1)	Z1,2	-4,12	-7,45	C5	0,0
Castellas (ZF1)	Z1,2	-0,15	-4,99	FR	0,0
Castellas (ZF1)	Z1,2	0,21	-5,98	C1	0,0
Castellas (ZF1)	Z1,2	0,39	-4,73	M	0,0
Castellas (ZF1)	Z1,2	0,61	-5,77	M	0,0
Castellas (ZF2)	Z2,2	0,58	-5,47	FR	0,0
Castellas (ZF2)	Z2,2	0,77	-5,38	C1	0,0
Castellas (ZF2)	Z2,2	0,92	-4,91	FR	0,0
Castellas (ZF2)	Z2,7	-4,38	-7,15	C5	0,0
Castellas (ZF2)	Z2,7	-3,97	-7,13	C5	0,0
Castellas (ZF2)	Z2,7	-3,78	-8,04	C5	0,0
Castellas (ZF2)	Z2,7	-3,56	-7,86	C5	0,0
Castellas (ZF2)	Z2,7	-3,24	-7,48	C5	0,0
Castellas (ZF2)	Z2,7	-3,23	-8,54	C5	0,0
Castellas (ZF2)	Z2,7	-3,18	-7,38	M	0,0
Castellas (ZF2)	Z2,7	-1,68	-5,63	FR	0,0
Castellas (ZF2)	Z2,7	-1,40	-9,52	C3	0,0
Castellas (ZF2)	Z2,7	-2,86	-6,03	FR	1,0
Castellas (ZF5)	Z5,4	0,27	-8,25	C3	0,0
Castellas (ZF5)	Z5,4	0,31	-7,87	C3	0,0
Castellas (ZF5)	Z5,4	0,32	-8,23	C3	0,0
Castellas (ZF5)	Z5,4	1,05	-7,13	FR	0,4
Castellas (ZF5)	Z5,4	1,06	-6,34	C1	0,4
Castellas (ZF5)	Z5,4	1,08	-6,76	C1	0,4
Castellas (ZF5)	Z5,4	1,37	-6,03	FR	0,4
Castellas (ZF5)	Z5,4	1,42	-6,15	FR	0,4
D19	3B	-0,81	-6,52	B	0,0
D19	3B	1,09	-5,20	B	0,0
D19	3B	-1,20	-6,50	C1	0,0
D19	3B	-1,02	-6,33	C1	0,0
D19	3B	0,11	-6,25	C1	0,0
D19	3B	-0,74	-6,23	M	0,0
D19	9	-2,32	-7,30	B	9,2
D19	13a	-3,44	-8,11	B	14,3
D19	13a	-2,96	-7,93	B	14,3
D19	13C	-2,97	-7,62	M	14,3
D19	13C	-2,86	-7,79	M	14,3
D19	13C	-2,70	-8,12	M	14,3

https://doi.org/10.5194/se-2019-153
Preprint. Discussion started: 28 October 2019

Solid Earth
Discussions

D19	13C	-2,67	-7,96	M	14,3
D19	13C	-2,66	-8,16	M	14,3
D19	13C	-2,50	-7,77	M	14,3
D19	13C	-1,54	-8,98	M	14,3
D19	17	-2,58	-7,68	B	18,7
D19	14A	-1,97	-6,38	B	18,7
D19	14A	-1,87	-6,74	B	18,7
D19	15B	-2,2	-7,4	B	18,7
D19	17	-1,05	-6,40	C1	18,7
D19	14A	-1,77	-6,74	C1	18,7
D19	14A	-2,42	-6,43	C4	18,7
D19	14A	-2,06	-6,67	C4	18,7
D19	21	-2,23	-6,54	B	24,4
D19	RSG	-1,90	-7,66	B	28,4
D19	RSG	-1,70	-7,83	B	28,4
D19	RSD	-2,87	-7,10	B	29,5
D19	RSD	-2,76	-7,14	B	29,5
D19	RSD	-0,93	-9,40	C3	29,5
D19	RSF1	-2,40	-7,28	B	34,7
D19	RSF2	-2,14	-7,39	B	34,7
D19	RSF2	-1,78	-7,27	B	34,7
D19	RSF1	-1,03	-9,44	C3	34,7
D19	RSF2	-1,93	-8,05	C3	34,7
D19	RSF2	-0,59	-9,40	C3	34,7
D19	RSF2	-2,95	-8,14	C4	34,7
D19	RSE 1	-2,53	-7,33	B	35,0
D19	RSE 2	-2,59	-7,41	B	35,0
D19	RSE 1	-1,71	-7,68	C3	35,0
D19	RSE 2	-1,84	-6,73	C3	35,0
D19	57	-2,07	-5,93	B	38,1
D19	57	-1,94	-5,87	B	38,1
D19	57	-1,83	-7,06	C3	38,1
D19	57	-1,10	-6,75	C3	38,1
D19	57	-4,02	-7,04	C4	38,1
D19	57	-2,17	-5,72	C4	38,1
D19	57	-1,58	-6,52	FR	38,1
D19	57	-7,20	-5,68	M	38,1
D19	57	-7,13	-5,90	M	38,1
D19	28b	-1,03	-7,21	B	39,3
D19	28b	-1,03	-6,10	C3	39,3
D19	28b	-4,09	-6,92	C4	39,3
D19	28b	-2,58	-7,40	C4	39,3
D19	28b	-2,47	-7,54	C4	39,3
D19	30a	-1,61	-7,04	B	42,6
D19	30a	-1,41	-6,87	B	42,6
D19	30a	-3,23	-7,03	C4	42,6

https://doi.org/10.5194/se-2019-153
Preprint. Discussion started: 28 October 2019

D19	30a	-2,89	-7,45	C4	42,6
D19	24a	-1,21	-7,52	B	51,1
D19	27b	-1,92	-7,48	B	57,9
D19	31	-1,24	-6,44	B	65,0
D19	32	-1,75	-7,50	B	67,4
D19	34	-1,79	-7,49	B	72,2
D19	36	-1,32	-7,21	B	77,8
D19	38	-1,73	-7,59	B	81,5
D19	62	-2,0	-7,6	B	86,0
D19	42	-0,81	-6,80	B	91,9
D19	63	-0,6	-5,5	B	124,0
D19	64	-1,2	-5,9	B	160,0
D19	65	-1,1	-6,6	B	197,0
D19	66	-1,3	-5,2	B	236,0
D19	60a	-3,06	-9,18	B	255,2
D19	60B	-4,80	-8,47	B	255,2
D19	60B	-4,66	-8,92	B	255,2
D19	61	-1,53	-9,87	C3	255,2
D19	61	-1,36	-9,89	C3	255,2
D19	60a	-1,15	-9,70	C3	255,2
D19	60a	-3,32	-9,11	C4	255,2
D19	60B	-5,10	-9,09	C4	255,2
D19	60B	-4,73	-8,84	C4	255,2
D19	60B	-4,15	-9,18	C4	255,2
D19	60B	-4,07	-9,16	C4	255,2
D19	60B	-2,90	-9,06	C4	255,2
D19	60a	-3,83	-7,85	M	255,2
D19	60B	-5,04	-9,17	M	255,2
D19	60B	-4,25	-8,14	M	255,2
D19	60B	-3,61	-8,58	M	255,2
D19	60B	-3,61	-8,13	M	255,2

-

IV. Diagenetic evolution of fault zones and impact on reservoir properties

The Urgonian carbonates in La Fare anticlinal undergone 3 important diagenetic events that impact the host rock and/or locally, only the fault zones. We discriminate diagenetic events occurring before and during faulting. Combined superposition, overlap, cross-cutting principles and isotopic signature of cements brought out the chronology between phases and revealed the paragenetic sequence (Fig. 7).

https://doi.org/10.5194/se-2019-153
Preprint. Discussion started: 28 October 2019

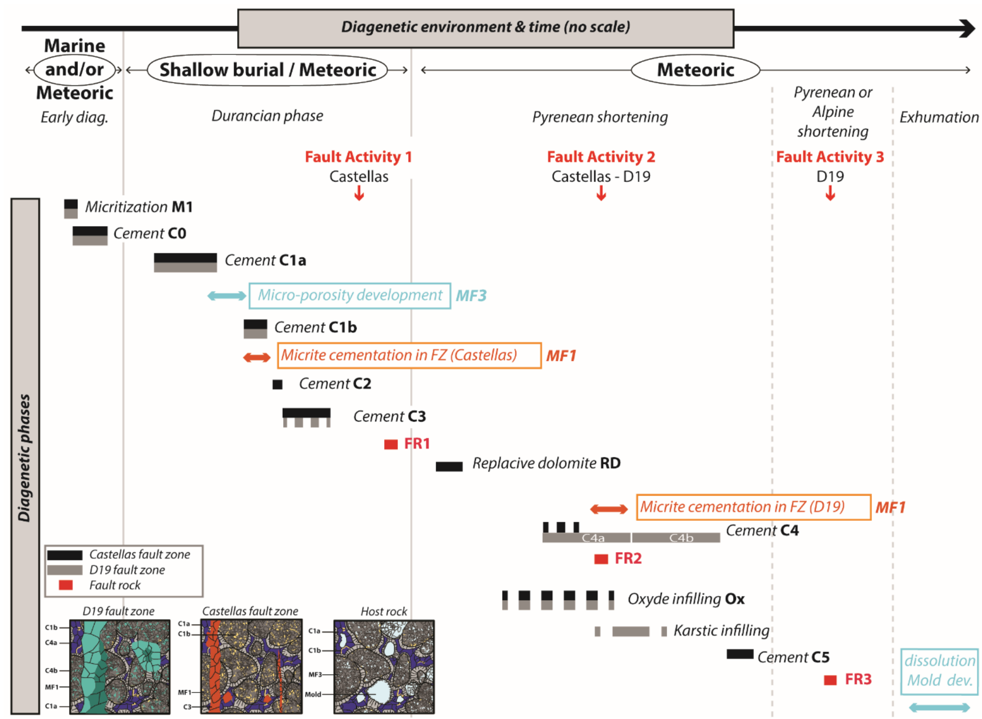

Figure 7: Paragenetic sequence of the both fault zones (black: Castellas, grey: D19) with micro-porosity development (blue) and cementation (orange) and fault zone activation (red).

1. Pre fault diagenesis – Micro-porosity development

During Upper Barremian and early after the deposition, micro-bores organisms at the sediment-water interface enhanced the formation of micritic calcitic envelopes on bioclasts, ooids and peloids (Purser, 1980; Reid and Macintyre, 2000; Samankassou et al., 2005; Vincent et al., 2007). This micritisation in marine conditions is typical for Urgonian low energy inner platform

https://doi.org/10.5194/se-2019-153
Preprint. Discussion started: 28 October 2019

Solid Earth
Discussions
Open Access
EGU

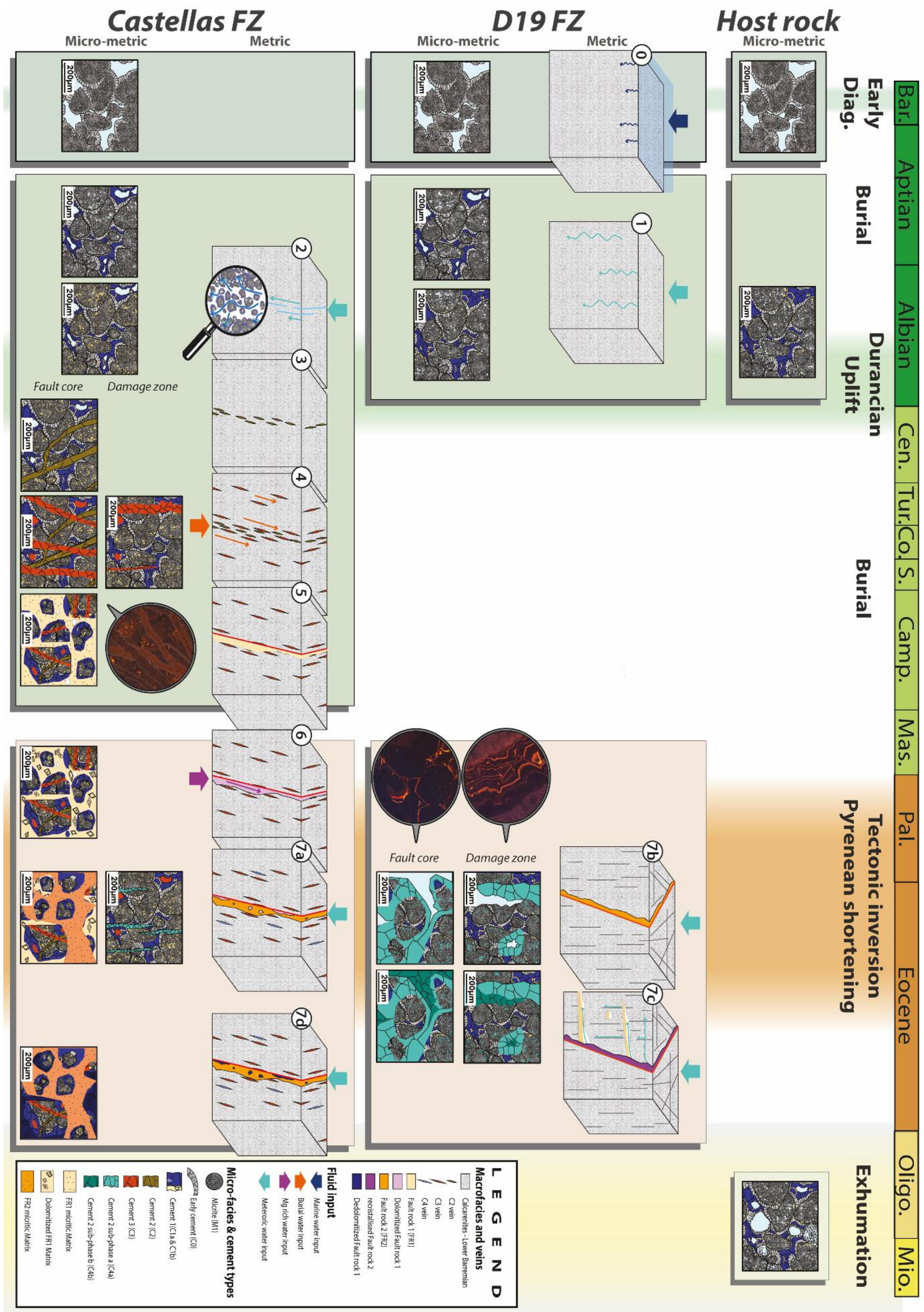

Figure 8 : Diagenetic and geodynamic evolution since the Barremian of both fault zones and host rock at the metric and micro-metric scale.

(Fournier et al., 2011; Masse, 1976). Subsequently, cement C0 formed around grains and created a solid shelve inducing the conservation of the clast shape during the later burial compaction (Step 0 on Fig. 8). However, the majority of isotopic values do not fit in the Barremian sea water calcite box which ranges from -1.00‰ to -4.00‰ for $\delta^{18}O$ and from +1.00‰ to +3.00‰ for $\delta^{13}C$ (Fouke et al., 1996; Godet et al., 2006). Only two values sampled in the micritised grains have isotopic values close to $\delta^{13}C$ and $\delta^{18}O$ of the Barremian sea water calcite. This depletion indicates the slight impact of C0 cementation on isotopic values.

The next sub-phase of cementation C1a partly fills intergranular porosity. This non luminescent cement with isotopic values ranging from -6.8‰ to -3.9‰ for $\delta^{18}O$ and from -1.0‰ to +1.3‰ for $\delta^{13}C$ is characteristic for mixed fluids. Léonide et al. (2014) measured a calcite cement S1, near La Fare anticline with similar luminescence and isotopic range values (mean: $\delta^{18}O$= −5.49‰; $\delta^{13}C$=+2.34‰). These authors linked this cementation phase to a shallow burial meteoric flow under equatorial climate during Durancian uplift. This diagenetic event led to micrite re-crystallization and development of microporosity (MF3). Since La fare Carbonates were exhumed at that time (Guyonnet-Benaize et al., 2010; Léonide et al., 2014) they undergone similar impact on their reservoir properties. Indeed, the meteoric fluids led to (Step 1 on Fig. 8):

(i) Cementation of C1a, partly filling intergranular porosity (Fig. 9B1a)
(ii) Micrite re-crystallization and microporosity MF3 setup by Ostwald ripening processes (Ostwald, 1886; Volery et al., 2010).

The micrite re-crystallization strongly increased rock porosity due to enhanced microporosity (Fig. 9B1b). Microporous limestones have a high matrix porosity but low to moderate matrix permeability (Deville de Periere et al., 2011; Jack and Sun, 2003). Indeed, in the case of Barremian limestones of La Fare anticline, porosity is >10% but located in the grains, what restricts possible flow pathways. Resulting from this event, Urgonian carbonates formed a type III reservoir *sensu* Nelson (2001).

2. Fault related diagenesis – Alteration of reservoir properties

a. Normal faulting-related diagenesis

The Castellas fault first nucleated during Durancian uplift (Aubert et al., 2019b; Matonti et al., 2012) impacting the host Urgonian carbonates. Fault nucleation mechanisms can lead to dilation processes (Main et al., 2000; Wilkins et al., 2007; Zhu and Wong, 1997) under low confining pressure (<100KPa; Alikarami & Torabi 2015). This is only possible in highly porous

https://doi.org/10.5194/se-2019-153
Preprint. Discussion started: 28 October 2019

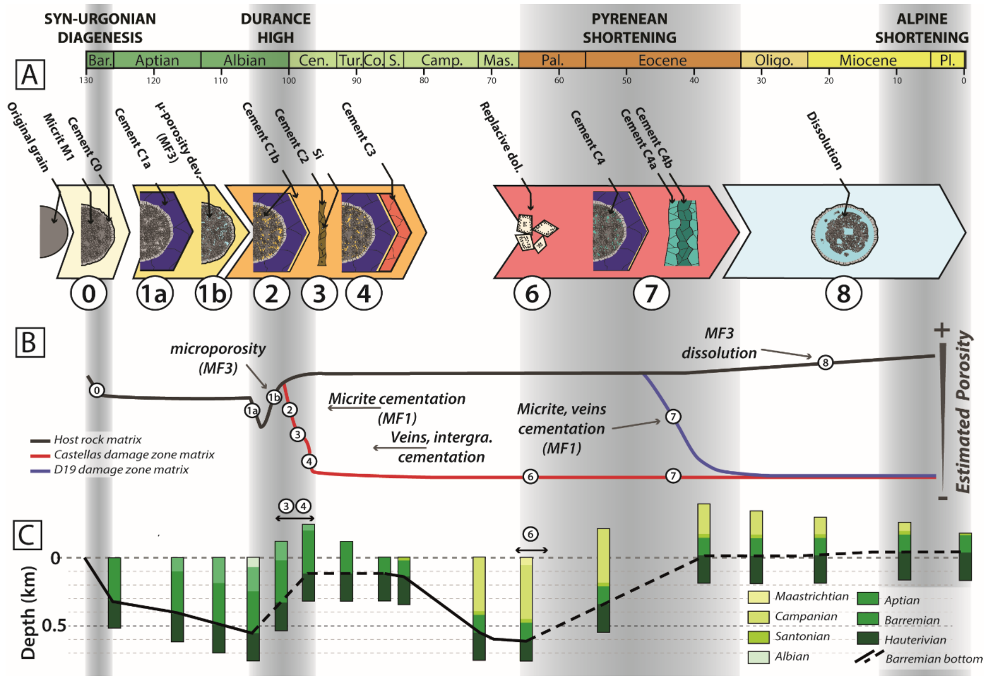

Figure 9 : Evolution of reservoir properties. different cementation phases; B: relative porosity evolution of the host rock and the 2 fault zones; C: Burial/Uplift curved of Barremian basement (modified from Matonti et al. (2012))

granular media (Fossen, 2016; Fossen and Bale, 2007). Dilatancy is more significant with non-angular grain (Alikarami and Torabi, 2015). Because this process leads to dilatancy, it increases the rock permeability (Alikarami and Torabi, 2015; Bernard et al., 2002) in the first stage of deformation bands (Heiland et al., 2001; Lothe et al., 2002) what allows fluids to flow. In the case of the Castellas fault zone, the fault has been shown to nucleate under low confining pressure, extensional stress pattern, at a depth <1km (*Lamarche et al.* 2012). The early diagenetic stages had led to a partial cementation of intergranular porosity. This allowed the grains to be preserved and the rock to become brittle. Micarelli et al. (2006) have shown that during early stages, fault zones in carbonates have a hydraulic behaviour comparable to deformation bands. In the Urgonian carbonates of La Fare sector, dilatant processes enhanced fluid circulation in the rock along the deformation bands and led to the cementation of C1b (Step 2 on Fig. 8). However, dilation bands are unstable and grain collapse occurs swiftly after the beginning of the deformation due to an increase in the loading stresses (Lothe et al., 2002). This explains why C1b does not fill all the intergranular porosity. Consequently, as all micritic grains in fault zone are cemented by C1b, the bulk isotopic measurements are strongly

https://doi.org/10.5194/se-2019-153
Preprint. Discussion started: 28 October 2019

influenced by C1 cement isotopic values. This is the explanation why in transect 3 the bulk isotopic values 30m apart from the fault (-5.1‰ for $\delta^{18}O$ and -0.5‰ for $\delta^{13}C$) are close to bulk isotopic values far from the fault plane (>100m; -6.0‰ for $\delta^{18}O$ and -0.7‰ for $\delta^{13}C$, Fig. 6A). The C1a and C1b led to a local rock embrittlement and to a porosity decrease by cementation of the microporosity.

During the first stages of fault evolution in low porosity limestones, intense fracturing of the fault zone predating fault core formation is known to increase the permeability (Micarelli et al., 2006). In the studied faults, the first brittle event allowed an Al-rich fluid to flow with micro-metric quartz grains in the barren fractures, and C2 to cement (Step 3 on Fig. 8). The Urgonian facies of the studied area are composed of pure carbonates without siliciclastic input. Quartz grains and Aluminium could have been reworked from surrounding formations. The rocks underlying the studied exposed Urgonian carbonates are limestones and dolostones. Albian and Aptian rocks are marly and sandy limestones, respectively (Anglada et al., 1977). Hence, Aptian layers are very likely to be the source of quartz. The fluids must have carried small grains of quartz from the Aptian sandy limestones via the fracture network. The Al enrichment of C2 could result from the erosion of Albian and Aptian deposits during the Durancian uplift (Guendon and Parron, 1985; Triat, 1982).

As the fault zone continues throwing and growing, a new fracture set affected the fault-zone, leading to new fluid circulation and cementation of C3 in veins and preserved intergranular porosity (Step 4 on Fig. 8). The $\delta^{18}O$ isotopic values of C3 range from -10.40‰ to -6.73‰ with $\delta^{13}C$ values between -2.09‰ and +1.22‰. The $\delta^{18}O$ isotopic values can be typical for either burial marine and/or burial meteoric fluids. In both cases, the depth of burial is less than 1km. Indeed, the formula of *Ali* (1995) allows calculating a range of fluid temperatures responsible for C3. We considered the following parameters:

- $\delta^{18}O$ isotopic values for C3: from -10.40 to -6.73‰
- isotopic range of values for the Barremian sea water: from -1.00 to -4.00‰ for $\delta^{18}O$ (Fouke et al., 1996; Godet et al., 2006)
- meteoric water: -4.0‰ for $\delta^{18}O$ (Robinson et al., 2002)
- temperature of initial fluids: 33°C to 34°C (Littler et al., 2011)

We calculated a C3 fluid temperature 40°C and 60°C. If we consider a geothermal gradient of 26.4°C per km (Ali, 1995) the depth of fluid source is less than 1km. The negative $\delta^{13}C$ values tend to indicate that it would rather be a meteoric fluid than a marine fluid.

https://doi.org/10.5194/se-2019-153
Preprint. Discussion started: 28 October 2019

In La Fare fault zones, burial fluids can have two origins: either descending and cemented at the calculated depth, or ascending up to low depth. As C3 cementation occurred during the Durancian uplift and denudation, C3 most probably did not cemented at high depth (Fig. 9C4). More probably, C3 fluids were meteoric burial fluid which were upwelled under tectonic stresses.

Resulting from this cementation, rocks in this zone tightened down to <5%. The porosity did not change since this event (Fig. 9 B5). Implicitly, the fault zone was a barrier to fluid flow, leading to a reservoir compartmentalization. The C3 fluid flow also occurred along fracture clusters of the D19 sector and led to vein formation.

In a later stage, the fault core formed and the fault plane *sensu-stricto* appeared, leading to FR1 breccia with a permeable matrix with quartz grains >100µm in size (Step 5 on Fig. 8). These grains either came from silica from C2 in veins describe above or from Aptian overlying rocks. C2 silica crystals in veins are scarce and smaller than 10µm. Thus, quartz grains may rather come from Aptian rocks like the quartz found in C2 veins. The presence of Aptian quartz in the fault core proves that the Castellas fault affected Aptian rocks, which have later been eroded during the Durancian uplift. Implicitly, the fault activity is dated as before total erosion of Aptian rocks. Uncemented breccias within the fault core form good fluid pathways (Billi et al., 2008; Delle Piane et al., 2016). In the studied fault, the formation of FR1 breccia allowed the fault core to act as a drain. However, the cemented surrounding host rocks constrained the drainage area of this high permeable conduit.

b. Tectonic Inversion – Castellas fault related dolomitization

At the onset of the Pyrenean shortening, compressive stresses lead to underground water upwelling through the permeable fault core. This fluid flow triggered the dolomitization of FR1 matrix (Step 6 on Fig. 8). This matrix-selective dolomitization can be favoured by several factors:

(i) The matrix has higher permeability than cemented clasts with a smaller grain size, hence a higher grain surface area;
(ii) This type of upwelling fluids, so-called “squeegee-type”, are short lived processes (Buschkuehle and Machel, 2002; Deming et al., 1990; Dorobek, 1989; Machel et al., 2000) not favourable for massive dolomitization;

https://doi.org/10.5194/se-2019-153
Preprint. Discussion started: 28 October 2019

(iii) Low temperature fluids, under 50°-80°C, enabled the preservation of FR1 clast initial structure. Contrarily, high temperature dolomitization tends to be destructive (Machel, 2004);

(iv) The tight surrounding host rock constrained high Mg fluid circulation to the fault core.

Gisquet et al. (2013) noticed similar fault related replacive dolomitization phase in the Etoile massif, 23km South-Est of the studied zones. They linked the dolomitization to compressive conditions during the early (Late Cretaceous) Pyrenean shortening. After these authors, the tectonic stress led to low temperature upwelling fluids Mg-enriched by the dissolution of underlying Jurassic dolomites. The Jurassic dolomites also occur in La Fare anticline. Since the fluids leading to dolomitization of fault core were low temperature and since dolomites occur underground, it is possible that the dolomitization in La Fare and in the Etoile massif were similar and synchronous. Matrix dolomitization can increase inter-crystalline and/or inter-particle porosity up to 13% but the later dolomite overgrowth reduce the porosity and permeability (Lucia, 2004; Machel, 2004; Saller and Henderson, 2001). Hence, the in the first stages of dolomitization, the fault core was an important drain. After the growth of dolomite crystals, the fault core turned to barrier (Fig. 9 (B6 & C6))

c. Sinistral tectonic inversion – meteoric alteration of reservoir properties

The ongoing tectonic inversion with increasing compressive stresses finally led to the Castellas fault sinistral reactivation and to the onset of D19 fault zone (Aubert et al., 2019b). Aubert et al. (2019a) has shown that this compression reactivated the pre-existing early N030° back-ground fractures (Step 7 on Fig. 8). This tectonic event lead to FR2 in fault cores but with specific diagenetic consequences. In the D19 fault zone, the fault nucleation and reactivation of back-ground fractures led to pluri-metric to kilometric fault surfaces with a permeable fault rock acting as drains and localizing the fluid flow (Aubert et al., 2019a). This fluid flow resulted in the cementation of C4a and C4b in veins and micritized grains (MF1, Step 7c on Fig. 8), what led to a strong porosity decrease in the fault zone (Fig. 9, B7 and C7). However, not all fractures were cemented by C4, so the fracture porosity/permeability was preserved. Therefore, the D19 fault zone became a type I reservoir sensu Nelson (2001) with a very low matrix porosity/permeability and high fracture permeability (Aubert et al., 2019a).

Along F2, successive fluids gave rise to karsts, karstic filling and dissolution/cementation of FR2 matrix (Step 7c on Fig. 8). Then, FR2 was sealed by C4 cementation. Isotopic values of

https://doi.org/10.5194/se-2019-153
Preprint. Discussion started: 28 October 2019

C4 (from -9.2 to -6.1‰ for $\delta^{18}O$ and from -5.01‰ to -1.0‰ for $\delta^{13}C$) highlight the strong influence of meteoric fluids. This is coherent with the occurrence of karstic fill due to fluid circulations in vadose zone, alternating dissolution and cementation (Swart, 2015). However, the positive covariance between $\delta^{18}O$ and $\delta^{13}C$ of C4 suggests mixed fluids (Allan and Matthews, 1982) of meteoric water and burial or marine water.

In the Castellas fault zone, the host rocks are slightly impacted by these meteoric fluid circulations. Yet, some veins filled with C4a occur along transect 2 and transect 3 (Step 7a on Fig. 8). Two samples have higher $\delta^{18}O$ and $\delta^{13}C$ isotopic values (respective mean of -6.25‰ and -4.2‰ for $\delta^{18}O$ -0.64 and -0.09‰ for $\delta^{13}C$) similar to C1 (Fig. 6A). This indicates that C4 in the Castellas fault zone was precocious in comparison to the D19. Cements C4 in Castellas area are restricted to transect 2. Transect 2 crosscut through the Castellas fault at the location of a relay zone (Fig. 2A). Relay or linkage zones occur where two fault segments overlap each other during fault grow (Kim et al., 2004; Long and Imber, 2011; Walsh et al., 1999, 2003). Consequently, the fault complexity, the fracture intensity and the fracture-strike range are increased (Kim et al., 2004; Sibson, 1996). This process in the studied area resulted in a well-connected fracture network that increased the local permeability and allowed local fluid circulations. In transect 2, the increase of the local permeability in the relay zone enhanced fluid flow related to cement C4. The relay zones along the Castellas fault and their consequences on the fracture permeability are, therefore, responsible for this local cementation event. Contrarily, cementation in D19 fault zone is linked to the highly permeable fault surfaces which acted as a drains (Aubert et al., 2019a). That implies that the cementation occurred only after the formation of the fault surface. In the case of Castellas, the relay zone was already present, inherited from the former normal activity, allowing early C4 fluid to flow in fault zone. This, in addition, explains why the early C4 cementation has not been recorded in D19 fault zone. The C4 cementation in T2 reduced the porosity to less than 8% on a larger zone (>60m) than in both others transects (T1 ≈30m, T3>40m).

The reactivation of the Castellas fault formed a new fracture network that locally triggerred the fracture connectivity and permeability. The Castellas fault zone formed a type I reservoir (Nelson, 2001), but lateral variation of the fracture network implies lateral variations of the hydraulic properties. Thus, the fault zone was both a drain and a barrier (Matonti et al., 2012), such as a sieve.

https://doi.org/10.5194/se-2019-153
Preprint. Discussion started: 28 October 2019

After these events, the matrix of the Castellas fault core was de-dolomitisation (FR1) in relation to cementation C5 (Step 7d on Fig. 8). The C5 cement isotope values (mean of -7.49‰ for $\delta^{18}O$ and -4.01‰ for $\delta^{13}C$) are comprised within C4 positive covariance between $\delta^{18}O$ and $\delta^{13}C$. This indicates a continuity between C4 and C5 fluid flows. The measurements with the SEM revealed a lack of Mg in the matrix indicating that C5 totally recrystallized the replacive dolomite. Following this de-dolomitization phase, no additional diagenetic event is recorded in Castellas fault zone.

A late Pyrenean to alpine compression reactivated the D19 fault zone what formed the new fault rock FR3. The matrix of this fault rock has very low $\delta^{13}C$ isotopic values (mean of -6.83‰) indicating an organic matter input (Swart, 2015). This implies soils, and thus results from a near surface fluid circulation. We deduce that the D19 faults was lately reactivated after the folding of the La Fare anticline. There is no such cementation with similar isotope values in the fault zone, meaning that fluids and cements did not alter the fault zone diagenetic properties.

Finally, the late exhumation of the Urgonian carbonate host rocks led to flows incurring dissolution of MF3 grains in the host rock. This phase triggered the moldic porosity and increased the porosity/permeability (Fig. 9 B8, C8). These flows, however, did not affect fault zones.

3. Evolution of fault zones reservoir properties

The host rock presents a monophasic evolution and switch from a type IV reservoir where matrix provided storage and flow, to a Type III reservoir where the fractures are pathways for flow but the production comes from the matrix (*Nelson* 2001, Fig. 10A). The fault zones present a more complex polyphase evolution than the host rock. Indeed, their reservoir properties evolved from a type IV reservoir corresponding to the host rock to a type I reservoir where fractures provide both storage and flow pathways (*Nelson* 2001,Fig. 10A). Both fault zones present slight differences. The Castellas fault zone was completely tight soon after C3 cementation. Consequently, it did not fit to the Nelson reservoir type classification. However, after fault core formation, the fault zone present a high fault core permeability. In this study we propose a new approach with a triangle diagram taking into account fault core permeability to remove the flaws of this method (Fig. 10B). Thus, for Castellas fault zone, the permeability evolve from the host rock permeability (100% matrix) to a permeability due to 50% to the matrix and 50% to the fault core during dilation band development (Fig. $10B_2$). Thereafter, during the two fracture events permeability is mainly link to fractures (C2: 30% FC, 70%

https://doi.org/10.5194/se-2019-153
Preprint. Discussion started: 28 October 2019

fractures; C3: 15% FC, 15% matrix, 70% fractures; Fig. $10B_{3,4}$). Then, after fault core formation and during dolomitization event, permeability is solely located in the fault core (Fig. $10B_{6,7}$). Lastly, after fault zone reactivation, the permeability is due to 20% to the FC and 80% to fractures (Fig. $10B_{7c}$). The D19 fault zone permeability during its development was related at 20% to the matrix, 20% to the fractures and 60% to the fault core (Fig. $10B_{7a\&b}$).

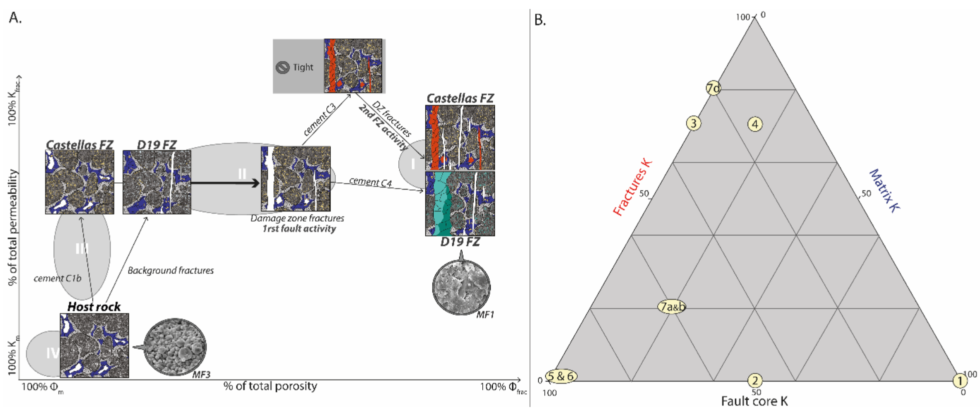

Figure 10 : Castellas and D19 fault zone reservoir properties evolution. A: evolution of permeability and porosity taking into account fault zone fractures and matrix after Nelson (2001) and B: Triangle diagram of permeability evolution with 3 components: matrix, fractures and fault core.

V. Conclusion

This study deciphered the diagenetic evolution of two fault zones and the impact on the reservoir properties of both fault and host rock in the frame of the overall geodynamic context of the SE basin. The main outcomes are:

- Fault zones may have a complex diagenetic history, but most diagenetic phases occur during the nucleation of the fault. In the case of Castellas fault zone, the diagenetic imprint is mainly influenced by early diagenesis occurring along fractures and diffuse dilation zones prior to the proper fault plane nucleation. Regarding D19 fault zone, most of diagenetic alterations occurred just after fault onset in the first stage of their activity. In both cases, the cementation altered initial reservoir properties in the fault zone vicinity, switching from type III to type I during the first stages of fault apparition. Later fault reactivation thinly impacts matrix porosity/permeability.
- Fault zones act as drains canalizing fluid flows in the beginning of their formation. This induces fault zone cementation but preservation of host rock microporosity. This

https://doi.org/10.5194/se-2019-153
Preprint. Discussion started: 28 October 2019

important fluid drainage is visible on D19 outcrop where the flows led to dissolution/cementation of fault rock matrix and formed karsts.

- All diagenetic stages, including cementation and dolomitization, result from low temperature flows with important meteoric water input. This low temperature disprove any hydrothermal influence. Therefore, both fault zones were not linked to high depth basement faults.

This regional study allows to draw broader rules for polyphase faults in granular carbonates at low depth (Fig.9).

- Under extensive context, fault nucleation can lead to dilation band acting as conduits for fluid flow. Carbonates are very sensitive to fluid and rock-fluids interactions. Thus, the onset of dilation bands triggers important diagenetic reactions that strongly alter local reservoir properties. During later fault zone development, the diagenesis depends on faults zones internal architecture.
- Fracture networks related to fault nucleation in granular carbonates form good fluid pathways before proper fault plane formation. However, in the case of pre-fractured carbonates, like D19 fault zone, fault rocks early appear in fault cores. In the later cases, fluids flowed preferentially within the permeable breccia rather than the damage zone fracture network.

https://doi.org/10.5194/se-2019-153
Preprint. Discussion started: 28 October 2019

Agosta, F., Prasad, M. and Aydin, A.: Physical properties of carbonate fault rocks, Fucino Basin (Central Italy): implications for fault seal in platform carbonates, Geofluids, 7, 19–32, doi:10.1111/j.1468-8123.2006.00158.x, 2007.

Agosta, F., Mulch, A., Chamberlain, P. and Aydin, A.: Geochemical traces of CO2-rich fluid flow along normal faults in central Italy, Geophys. J. Int., 174(2), 1074–1096, doi:10.1111/j.1365-246X.2008.03792.x, 2008.

Agosta, F., Alessandroni, M., Antonellini, M., Tondi, E. and Giorgioni, M.: From fractures to flow: A field-based quantitative analysis of an outcropping carbonate reservoir, Tectonophysics, 490(3–4), 197–213, doi:10.1016/j.tecto.2010.05.005, 2010.

Agosta, F., Ruano, P., Rustichelli, A., Tondi, E., Galindo-Zaldívar, J. and Sanz de Galdeano, C.: Inner structure and deformation mechanisms of normal faults in conglomerates and carbonate grainstones (Granada Basin, Betic Cordillera, Spain): Inferences on fault permeability, J. Struct. Geol., 45, 4–20, doi:10.1016/j.jsg.2012.04.003, 2012.

Ali, Y.: Carbonate cement stratigraphy and timing of diagenesis in a Miocene mixed carbonate-elastic sequence , offshore Sabah , Malaysia : constraints from cathodoluminescence , geochemistry , and isotope studies, , 99, 191–214, doi:10.1016/0037-0738(95)00044-9, 1995.

Alikarami, R. and Torabi, A.: Geomechanics for Energy and the Environment Micro-texture and petrophysical properties of dilation and compaction shear bands in sand, Geomech. Energy Environ., 3, 1–10, doi:10.1016/j.gete.2015.06.001, 2015.

Allan, J. R. and Matthews, R. K.: Isotope signatures associated with early meteoric diagenesis, Sedimentology, 29(6), 797–817, doi:10.1111/j.1365-3091.1982.tb00085.x, 1982.

Allmendinger, R. W., Cardozo, N. and Fisher, D. M.: Structural geology algorithms: Vectors and tensors, Cambridge Univ. Press, 9781107012, 1–289, doi:10.1017/CBO9780511920202, 2013.

Anglada, R., Arlhac, P., Catzigras, F., Colomb, E., Damiani, L., Durand, J. P., Durozoy, G., Guieu, G., Masse, J. P., Nury, D., Philip, J., Rouire, J., Rousset, C., Roux, R. M. and Blanc, J. J.: Notice explicative. Carte géologique de la France a 1/50 000. Martigues - Marseille., 1977.

Aubert, I., Lamarche, J. and Léonide, P.: Deciphering background fractures from damage fractures in fault zones and their effect on reservoir properties in microporous carbonates

(Urgonian limestones, SE France), Pet. Geosci., doi:DOI10.1144/petgeo2019-010, 2019a.

Aubert, I., Lamarche, J., Richard, P. and Leonide, P.: Imbricated Structure and Hydraulic Path Induced by Strike Slip Reactivation of a Normal Fault in Carbonates, in Fifth International Conference on Fault and Top Seals, p. 4., 2019b.

Bense, V. F., Gleeson, T., Loveless, S. E., Bour, O. and Scibek, J.: Fault zone hydrogeology, Earth-Science Rev., 127, 171–192, doi:10.1016/j.earscirev.2013.09.008, 2013.

Bernard, X. Du, Eichhubl, P. and Aydin, A.: Dilation bands : A new form of localized failure in granular media, , 29(24), 1–4, doi:10.1029/2002GL015966, 2002.

Besson, D.: Architecture du bassin rhodano-provençal miocène (Alpes , SE France) : relations entre déformation , physiographie et sédimentation dans un bassin molassique d ' avant-pays, Ecole des Mines, Paris., 2005.

Bestani, L.: Géométrie et cinématique de l'avant-pays provençal : Modélisation par coupes équilibrées dans une zone à tectonique polyphasée., Aix-Marseille University., 2015.

Bestani, L., Espurt, N., Lamarche, J., Bellier, O. and Hollender, F.: Reconstruction of the Provence Chain evolution, Southeastern France., Tectonics, 35, 1506–1525, doi:10.1002/2016TC004115, 2016.

Billi, A., Primavera, P., Soligo, M. and Tuccimei, P.: Minimal mass transfer across dolomitic granular fault cores, Geochemistry, Geophys. Geosystems, 9(1), doi:10.1029/2007GC001752, 2008.

Borgomano, J., Masse, J., Maskiry, S. Al, Borgomano, J. and International, S.: The lower Aptian Shuaiba carbonate outcrops in Jebel Akhdar, northern Oman: Impact on static modeling for Shuaiba petroleum reservoirs., Bull. Am. Assoc. Pet. Geol., 9(9), 1513–1529, doi:10.1306/61EEDCE2-173E-11D7-8645000102C1865D, 2002.

Borgomano, J., Masse, J. P., Fenerci-Masse, M. and Fournier, F.: Petrophysics of lower cretaceous platform carbonate outcrops in provence (SE France): Implications for carbonate reservoir characterisation, J. Pet. Geol., 36(1), 5–41, doi:10.1111/jpg.12540, 2013.

Bruna, P., Guglielmi, Y., Viseur, S., Lamarche, J. and Bildstein, O.: Coupling fracture facies with in-situ permeability measurements to generate stochastic simulations of tight carbonate aquifer properties : Example from the Lower Cretaceous aquifer , Northern Provence , SE

https://doi.org/10.5194/se-2019-153
Preprint. Discussion started: 28 October 2019

France, J. Hydrol., 529, 737–753, doi:10.1016/j.jhydrol.2015.08.054, 2015.

Buschkuehle, B. E. and Machel, H. G.: Diagenesis and paleo fluid flow in the Devonian Southesk-Cairn carbonate complex in Alberta , Canada, Mar. Pet. Geol., 19, 219–227, doi:10.1016/S0264-8172(02)00014-4, 2002.

Caine, J. S., Evans, J. P. and Forster, C. B.: Fault zone architechture and permeability structure, Geology, 24(11), 1025–1028, doi:10.1130/0091-7613(1996)024<1025, 1996.

Cardozo, N. and Allmendinger, N. W.: Sperical projections with OSXStereonets, Comput. Geosci., 51, 193–205, doi:10.1016/j.cageo.2012.07.021, 2013.

Champion, C., Choukroune, P. and Clauzon, G.: La déformation post-miocène en provence occidentale, Geodin. Acta, 13(2–3), 67–85, doi:10.1080/09853111.2000.11105365, 2000.

Chester, F. M. and Logan, J. M.: Implications for Mechanical Properties of Brittle Faults from Observations of the Punchbowl Fault Zone, California, PAGEOPH, 124(1/2), 79, doi:10.1007/BF00875720, 1986.

Chester, F. M. and Logan, J. M.: Composite planar fabric of gouge from the Punchbowl Fault, California, J. Struct. Geol., 9(5–6), doi:10.1016/0191-8141(87)90147-7, 1987.

Delle Piane, C., Giwelli, A., Clennell, M. Ben, Esteban, L., Nogueira Kiewiet, M. C. D., Kiewiet, L., Kager, S. and Raimon, J.: Frictional and hydraulic behaviour of carbonate fault gouge during fault reactivation — An experimental study, Tectonophysics, 690(PartA), 21–34, doi:10.1016/j.tecto.2016.07.011, 2016.

Deming, D., Nunn, A. and Evans, D. G.: Thermal Effects of Compaction-Driven Groundwater Flow, , 95(89), 6669–6683, doi:10.1029/JB095iB05p06669, 1990.

Demory, F. R., Conesa, G. I., Oudet, J. U., Mansouri, H. A. and Münch, P. H.: Magnetostratigraphy and paleoenvironments in shallow-water carbonates : The Oligocene-Miocene sediments of the northern margin of the Liguro- Provençal basin (West Marseille , southe ..., Bull. Soc. géol. Fr., 1, 37–55, doi:10.2113/gssgfbull.182.1.37, 2011.

Deville de Periere, M., Durlet, C., Vennin, E., Lambert, L., Bourillot, R., Caline, B. and Poli, E.: Morphometry of micrite particles in cretaceous microporous limestones of the middle east: Influence on reservoir properties, Mar. Pet. Geol., 28(9), 1727–1750, doi:10.1016/j.marpetgeo.2011.05.002, 2011.

Deville de Periere, M., Durlet, C., Vennin, E., Caline, B., Boichard, R. and Meyer, A.: Influence of a major exposure surface on the development of microporous micritic limestones - Example of the Upper Mishrif Formation (Cenomanian) of the Middle East, Sediment. Geol., 353, 96–113, doi:10.1016/j.sedgeo.2017.03.005, 2017.

Dorobek, S.: migration of erogenic fluids through the Siluro-Devonian Helderberg Group during late Paleozoic deformation : constraints on fluid sources and implications for thermal histories of sedimentary basins presence, , 159, 25–45, doi:10.1016/0040-1951(89)90168-6, 1989.

Eltom, H. A., Gonzalez, L. A., Hasiotis, S. T., Rankey, E. C. and Cantrell, D. L.: Paleogeographic and paleo-oceanographic influences on carbon isotope signatures: Implications for global and regional correlation, Middle-Upper Jurassic of Saudi Arabia, Sediment. Geol., 364, 89–102, doi:10.1016/j.sedgeo.2017.12.011, 2018.

Espurt, N., Hippolyte, J. C., Saillard, M. and Bellier, O.: Geometry and kinematic evolution of a long-living foreland structure inferred from field data and cross section balancing, the Sainte-Victoire System, Provence, France, Tectonics, 31(4), doi:10.1029/2011TC002988, 2012.

Evans, J. P., Forster, C. B. and Goddard, J. V.: Permeability of fault-related rocks, and implications for hydraulic structure of fault zones, J. Struct. Geol., 19(11), 1393–1404, doi:10.1016/S0191-8141(97)00057-6, 1997.

Ferraro, F., Agosta, F., Ukar, E., Grieco, D. S., Cavalcante, F., Belviso, C. and Prosser, G.: Structural diagenesis of carbonate fault rocks exhumed from shallow crustal depths: An example from the central-southern Apennines, Italy, J. Struct. Geol., 122(February), 58–80, doi:10.1016/j.jsg.2019.02.008, 2019.

Florida, S., Maliva, R. G., Missimer, T. M., Clayton, E. A. and Dickson, J. A. D.: Diagenesis and porosity preservation in Eocene microporous limestones , Sediment. Geol., 217(1–4), 85–94, doi:10.1016/j.sedgeo.2009.03.011, 2009.

Ford, M., Duchene, S., Gasquet, D. and Vanderhaeghe, O.: Two-phase orogenic convergence in the external and internal SW Alps, J. Geol. Soc. London., 163(5), 815–826, doi:10.1144/0016-76492005-034, 2006.

Fossen, H.: Structural geology, 2nd Editio., Cambridge University Press., 2016.

Fossen, H. and Bale, A.: Deformation bands and their influence on fluid flow, , 12(12), 1685–1700, doi:10.1306/07300706146, 2007.

Fouke, B. W., Everts, A. W., Zwart, E. W. and Schlager, W.: Subaerial exposure unconformities on the Vercors carbonate platform (SE France) and their sequence stratigraphic significance, Geol. Soc. London, Spec. Publ., 104, 295–319, 1996.

Fournier, F. and Borgomano, J.: Critical porosity and elastic properties of microporous mixed carbonate-siliciclastic rocks, Geophysics, 74(2), E93–E109, doi:10.1190/1.3043727, 2009.

Fournier, F., Leonide, P., Biscarrat, K., Gallois, A., Borgomano, J. and Foubert, A.: Elastic properties of microporous cemented grainstones, Geophysics, 76(6), E211–E226, doi:10.1190/geo2011-0047.1, 2011.

Gattacceca, J., Deino, A., Rizzo, R., Jones, D. S., Henry, B., Beaudoin, B. and Vadeboin, F.: Miocene rotation of Sardinia: New paleomagnetic and geochronological constraints and geodynamic implications, Earth Planet. Sci. Lett., 258(3–4), 359–377, doi:10.1016/j.epsl.2007.02.003, 2007.

Gisquet, F., Lamarche, J., Floquet, M., Borgomano, J., Masse, J. P. and Caline, B.: Three-dimensional structural model of composite dolomite bodies in folded area (upper jurassic of the Etoile massif, southeastern France), Am. Assoc. Pet. Geol. Bull., 97(9), 1477–1501, doi:10.1306/04021312016, 2013.

Godet, A., Bodin, S., Föllmi, K. B., Vermeulen, J., Gardin, S., Fiet, N., Adatte, T., Berner, Z., Stüben, D. and van de Schootbrugge, B.: Evolution of the marine stable carbon-isotope record during the early Cretaceous: A focus on the late Hauterivian and Barremian in the Tethyan realm, Earth Planet. Sci. Lett., 242(3–4), 254–271, doi:10.1016/j.epsl.2005.12.011, 2006.

Guendon, J.-L. and Parron, C.: Les phenomenes karstiques dans les processus de la bauxitisation sur substrat carbonate. Exemple de gisement du sud est de la France, Ann. la Société Géologique Belgique, 108, 85–92, 1985.

Guieu, G.: Un exemple de tectonique tangentielle: l'évolution du cadre montagneux de Marseille., Bull. la Société Géologique Fr., 7 (T.IX N°, 610–630, 1967.

Guyonnet-Benaize, C., Lamarche, J., Masse, J. P., Villeneuve, M. and Viseur, S.: 3D structural modelling of small-deformations in poly-phase faults pattern. Application to the Mid-

Cretaceous Durance uplift, Provence (SE France), J. Geodyn., 50(2), 81–93, doi:10.1016/j.jog.2010.03.003, 2010.

Hammond, K. J. and Evans, J. P.: Geochemistry , mineralization , structure , and permeability of a normal- fault zone , Casino mine , Alligator Ridge district , north central Nevada, , 25, 717–736, doi:10.1016/S0191-8141(02)00060-3, 2003.

Heiland, J., Raab, S. and Potsdam, G.: Experimental Investigation of the Influence of Differential Stress on Permeability of a Lower Permian (Rotliegend) Sandstone Deformed in the Brittle Deformation, Phys. Chem. earth, 26(1), 33–38, doi:10.1016/S1464-1895(01)00019-9, 2001.

Hodson, K. R., Crider, J. G. and Huntington, K. W.: Temperature and composition of carbonate cements record early structural control on cementation in a nascent deformation band fault zone: Moab Fault, Utah, USA, Tectonophysics, 690, 240–252, doi:10.1016/j.tecto.2016.04.032, 2016.

Hollis, C., Vahrenkamp, V., Tull, S., Mookerjee, A. and Taberner, C.: Pore system characterisation in heterogeneous carbonates : An alternative approach to widely-used rock-typing methodologies, Mar. Pet. Geol., 27(4), 772–793, doi:10.1016/j.marpetgeo.2009.12.002, 2010.

Jack, A. and Sun, S.: Controls on Recovery Factor in Fractured Reservoirs: Lessons Learned from 100 Fractured Fields, Proc. SPE Annu. Tech. Conf. Exhib., doi:10.2523/84590-MS, 2003.

Kim, Y. S., Peacock, D. C. P. and Sanderson, D. J.: Fault damage zones, J. Struct. Geol., 26(3), 503–517, doi:10.1016/j.jsg.2003.08.002, 2004.

Knipe, R. J.: The influence of fault zone processes and diagenesis on fluid flow, Diagenes. basin Dev. AAPG Stud. Geol., 36, 135–154 [online] Available from: http://archives.datapages.com/data/specpubs/resmi1/data/a067/a067/0001/0100/0135.htm, 1993.

Knipe, R. J., Jones, G. and Fisher, Q. J.: Faulting, fault sealing and fluid flow in hydrocarbon reservoirs: an introduction, Geol. Soc. London, Spec. Publ., 147(1), NP LP-NP, doi:10.1144/GSL.SP.1998.147.01.21, 1998.

Lamarche, J., Lavenu, A. P. C., Gauthier, B. D. M., Guglielmi, Y. and Jayet, O.: Relationships between fracture patterns, geodynamics and mechanical stratigraphy in Carbonates (South-East Basin, France), Tectonophysics, 581, 231–245, doi:10.1016/j.tecto.2012.06.042, 2012.

Lambert, L., Durlet, C., Loreau, J. P. and Marnier, G.: Burial dissolution of micrite in Middle East carbonate reservoirs (Jurassic-Cretaceous): Keys for recognition and timing, Mar. Pet. Geol., 23(1), 79–92, doi:10.1016/j.marpetgeo.2005.04.003, 2006.

Laubach, S. E., Eichhubl, P., Hilgers, C. and Lander, R. H.: Structural diagenesis, J. Struct. Geol., 32(12), 1866–1872, doi:10.1016/j.jsg.2010.10.001, 2010.

Lavenu, A. P. C., Lamarche, J., Gallois, A. and Gauthier, B. D. M.: Tectonic versus diagenetic origin of fractures in a naturally fractured carbonate reservoir analog [Nerthe anticline, Southeastern France, Am. Assoc. Pet. Geol. Bull., 97(12), 2207–2232, doi:10.1306/04041312225, 2013.

Leonide, P., Borgomano, J., Masse, J. and Doublet, S.: Relation between stratigraphic architecture and multi-scale heterogeneities in carbonate platforms : The Barremian – lower Aptian of the Monts de Vaucluse , SE France, Sediment. Geol., 265–266, 87–109, doi:10.1016/j.sedgeo.2012.03.019, 2012.

Léonide, P., Fournier, F., Reijmer, J. J. G., Vonhof, H., Borgomano, J., Dijk, J., Rosenthal, M., Van Goethem, M., Cochard, J. and Meulenaars, K.: Diagenetic patterns and pore space distribution along a platform to outer-shelf transect (Urgonian limestone, Barremian-Aptian, SE France), Sediment. Geol., 306, 1–23, doi:10.1016/j.sedgeo.2014.03.001, 2014.

Littler, K., Robinson, S. A., Bown, P. R., Nederbragt, A. J. and Richard, D.: High sea-surface temperatures during the Early Cretaceous Epoch, Nat. Geosci., 4(3), 169–172, doi:10.1038/ngeo1081, 2011.

Long, J. J. and Imber, J.: Geological controls on fault relay zone scaling, J. Struct. Geol., 33(12), 1790–1800, doi:10.1016/j.jsg.2011.09.011, 2011.

Lothe, A. E., Gabrielsen, R. H., Hagen, N. B. and Larsen, B. T.: An experimental study of the texture of deformation bands : e ff ects on the porosity and permeability of sandstones, , (1990), doi:10.1144/petgeo.8.3.195, 2002.

Lucia, F. J.: Origin and petrophysics of dolostone pore space, Geom. Petrog. Dolomite Hydrocarb. Reserv. Geol. Soc. London, Spec. Publ., 235, 141–155,

https://doi.org/10.5194/se-2019-153
Preprint. Discussion started: 28 October 2019

doi:10.1144/GSL.SP.2004.235.01.06, 2004.

Machel, H. G.: Concepts and models of dolomitization: a critical reappraisal, Geol. Soc. London, Spec. Publ., 235(1), 7–63, doi:10.1144/GSL.SP.2004.235.01.02, 2004.

Machel, H. G., Cavell, P. A., Buschkuehle, B. E. and Michael, K.: Tectonically induced fluid flow in Devonian carbonate aquifers of the Western Canada Sedimentary Basin, ournal geochemical Explor., 70, 213–217, doi:10.1016/S0375-6742(00)00093-5, 2000.

Main, I. G., Kwon, O., Ngwenya, B. T. and Elphick, S. G.: Fault sealing during deformation-band growth in porous sandstone, Geology, 28(12), 1131–1134, doi:10.1130/0091-7613(2000)28<1131:FSDDGI>2.0.CO;2, 2000.

Masse, J.-P. and Philip, J.: Paléogéographie et tectonique du Crétacé moyen en Provence: révision du concept d'isthme durancien., Rev. Géographie Phys. Géologie Dyn., 18(1), 49–46, 1976.

Masse, J. P.: Les calcaires urgoniens de Provence (Valanginien-Aptien Inférieur) - Stratigraphie, paléontologie, paléoenvironnements et leur évolution., Marseille, Thèse de la Faculté des Sciences de Luminy (U2)., 1976.

Masse, J. P. and Fenerci-Masse, M.: Carbonate production by rudist bivalves. The record of Late Barremian requieniid communities from Provence (SE France), Palaeogeogr. Palaeoclimatol. Palaeoecol., 234(2–4), 239–257, doi:10.1016/j.palaeo.2005.10.010, 2006.

Masse, J. P. and Fenerci Masse, M.: Drowning discontinuities and stratigraphic correlation in platform carbonates. The late Barremian-early Aptian record of southeast France, Cretac. Res., 32(6), 659–684, doi:10.1016/j.cretres.2011.04.003, 2011.

Matonti, C., Lamarche, J., Guglielmi, Y. and Marié, L.: Structural and petrophysical characterization of mixed conduit/seal fault zones in carbonates: Example from the Castellas fault (SE France), J. Struct. Geol., 39, 103–121, doi:10.1016/j.jsg.2012.03.003, 2012.

Micarelli, L., Benedicto, A. and Wibberley, C. A. J.: Structural evolution and permeability of normal fault zones in highly porous carbonate rocks, J. Struct. Geol., 28(7), 1214–1227, doi:10.1016/j.jsg.2006.03.036, 2006.

Molli, G., Cortecci, G., Vaselli, L., Ottria, G., Cortopassi, A., Dinelli, E., Mussi, M. and Barbieri, M.: Fault zone structure and fluid–rock interaction of a high angle normal fault in

Carrara marble (NW Tuscany, Italy) // Fault zone structure and fluid–rock interaction of a high angle normal fault in Carrara marble (NW Tuscany, Italy), J. Struct. Geol., 32(9), 1334–1348, doi:10.1016/j.jsg.2009.04.021, 2010.

Molliex, S., Bellier, O., Terrier, M., Lamarche, J., Martelet, G. and Espurt, N.: Tectonic and sedimentary inheritance on the structural framework of Provence (SE France): Importance of the Salon-Cavaillon fault, Tectonophysics, 501(1–4), 1–16, doi:10.1016/j.tecto.2010.09.008, 2011.

Moss, S. and Tucker, M. E.: Diagenesis of Barremian-Aptian platform carbonates (the Urgonian Limestone Formation of SE France): near-surface and shallow-burial diagenesis, Sedimentology, 42(6), 853–874, doi:10.1111/j.1365-3091.1995.tb00414.x, 1995.

Nelson, R.: Geologic Analysis of Naturally Fractured Reservoirs, second ed., 2001.

Ostwald, W.: Lehrbuch der allgemeinen Chemie, Verlag von Wilhelm Engelmann, Leipzig, 2, 909, 1886.

Philip, J.: Les formations calcaires à rudistes du Crétacé supérieur provençal et rhodanien. Thèse de Doctorat, Université de Provence (Marseille)., 1970.

Le Pichon, X., Bergerat, F. and Roulet, M.-J.: Plate kinematics and tectonics leading to the Alpine belt formation; A new analysis, Geol. Soc. Am., 218(March 1986), 111–131, doi:10.1130/SPE218-p111, 1988.

Pichon, X. Le, Rangin, C., Hamon, Y., Loget, N., Lin, J. Y., Andreani, L. and Flotte, N.: Geodynamics of the france southeast basin, Bull. la Soc. Geol. Fr., 181(6), 477–501, doi:10.2113/gssgfbull.181.6.477, 2010.

Purser, B. H.: Sédimentation et diagenèse des carbonates néritiques récents, Les éléments de la sédimentation et de la diagenèse, Ed. Tech., 1, 366, 1980.

Reches, Z. and Dewers, T. A.: Gouge formation by dynamic pulverization during earthquake rupture, Earth Planet. Sci. Lett., 235(1–2), 361–374, doi:10.1016/j.epsl.2005.04.009, 2005.

Reid, R. P. and Macintyre, I. G.: Microboring Versus Recrystallization: Further Insight into the Micritization Process, J. Sediment. Res., 70(May), 24–28, doi:10.1306/2DC408FA-0E47-11D7-8643000102C1865D, 2000.

Robinson, S. A., Robinson, S. A., Andrews, J. E., Hesselbo, S. P., Radley, J. D., Dennis, P. F., Harding, I. A. N. C. and Allen, P.: Atmospheric pCO2 and depositional environment from stable-isotope geochemistry of calcrete nodules (Barremian , Lower Cretaceous , Wealden Atmospheric p CO 2 and depositional environment from stable-isotope geochemistry of calcrete nodules (Barremian , J. Geol. Soc. London, 159, 215–224, doi:10.1144/0016-764901-015, 2002.

Roche, V.: Analyse structurale et géo-mécanique de réseau de failles du chaînon de La Fare les Oliviers (Provence), Univ. Montpellier 2, 45, 2008.

Rossetti, F., Aldega, L., Tecce, F., Balsamo, F., Billi, A. and Brilli, M.: Fluid flow within the damage zone of the Boccheggiano extensional fault (Larderello-Travale geothermal field, central Italy): Structures, alteration and implications for hydrothermal mineralization in extensional settings, Geol. Mag., 148(4), 558–579, doi:10.1017/S001675681000097X, 2011.

Saller, A. H. and Henderson, N.: Distribution of Porosity and Permeability in Platform Dolomites : Insight from the Permian of West Texas : reply, Am. Assoc. Pet. Geol. Bull., 85, 530–532, doi:10.1306/090800850530, 2001.

Sallier, B.: Carbonates microporeux : influence de l'architecture du milieu poreux et de la mouillabilité sur les écoulements diphasiques dans les réservoirs pétroliers., Univ. Genève., 2005.

Samankassou, E., Tresch, J. and Strasser, A.: Origin of peloids in Early Cretaceous deposits, Dorset, South England, Facies, 51(1–4), 264–273, doi:10.1007/s10347-005-0002-8, 2005.

Séranne, M.: The Gulf of Lion continental margin (NW Mediterranean) revisited by IBS: an overview, Geol. Soc. London, Spec. Publ., 156(1), 15–36, doi:10.1144/GSL.SP.1999.156.01.03, 1999.

Sibley, D. F. and Gregg, J. A. Y. M.: Classification of Dolomite Rock Texture, J. Sediment. Petrol., 57(6), 967–975, doi:10.1306/212F8CBA-2B24-11D7-8648000102C1865D, 1987.

Sibson, R. H.: Crustal stress, faulting and fluid flow, Geol. Soc. London, Spec. Publ., 78(1), 69–84, doi:10.1144/GSL.SP.1994.078.01.07, 1994.

Sibson, R. H.: Structural permeability of fluid-driven fault-fracture meshes, J. Struct. Geol., 18(8), 1031–1042, doi:10.1016/0191-8141(96)00032-6, 1996.

https://doi.org/10.5194/se-2019-153
Preprint. Discussion started: 28 October 2019

Sinisi, R., Petrullo, A. V., Agosta, F., Paternoster, M., Belviso, C. and Grassa, F.: Contrasting fault fluids along high-angle faults: a case study from Southern Apennines (Italy), Tectonophysics, 690(PartA), 206–218, doi:10.1016/j.tecto.2016.07.023, 2016.

Solum, J. G. and Huisman, B. A. H.: Toward the creation of models to predict static and dynamic fault-seal potential in carbonates, Pet. Geosci., 23(1), 70–91, doi:10.1144/petgeo2016-044, 2016.

Solum, J. G., Davatzes, N. C. and Lockner, D. A.: Fault-related clay authigenesis along the Moab Fault : Implications for calculations of fault rock composition and mechanical and hydrologic fault zone properties, J. Struct. Geol., 32(12), 1899–1911, doi:10.1016/j.jsg.2010.07.009, 2010.

Swart, P. K.: The geochemistry of carbonate diagenesis: The past, present and future, Sedimentology, 62(5), 1233–1304, doi:10.1111/sed.12205, 2015.

Tempier, C.: Modèle nouveau de mise en place des structures provençales, Bull. la Soc. Geol. Fr., 3, 533–540, doi:10.2113/gssgfbull.III.3.533, 1987.

Tondi, E.: Nucleation, development and petrophysical properties of faults in carbonate grainstones: Evidence from the San Vito Lo Capo peninsula (Sicily, Italy), J. Struct. Geol., 29(4), 614–628, doi:10.1016/j.jsg.2006.11.006, 2007.

Triat, J.: Paléoaltérations dans le crétacé supérieur de Provence rhodanienne, Strasbourg : Institut de Géologie – Université Louis-Pasteur., 1982.

Vincent, B., Emmanuel, L., Houel, P. and Loreau, J. P.: Geodynamic control on carbonate diagenesis: Petrographic and isotopic investigation of the Upper Jurassic formations of the Paris Basin (France), Sediment. Geol., 197(3–4), 267–289, doi:10.1016/j.sedgeo.2006.10.008, 2007.

Volery, C., Davaud, E., Foubert, A. and Caline, B.: Shallow-marine microporous carbonatereservoir rocks in the Middle East : relationship with seawater Mg/Ca ration and eustatic sea level, J. Pet. Geol., 32(October), 313–325, doi:10.1111/j.1747-5457.2009.00452.x, 2009.

Volery, C., Davaud, E., Foubert, A. and Caline, B.: Lacustrine microporous micrites of the Madrid Basin (Late Miocene, Spain) as analogues for shallow-marine carbonates of the Mishrif reservoir formation (Cenomanian to Early Turonian, Middle East), Facies, 56(3), 385–397,

https://doi.org/10.5194/se-2019-153
Preprint. Discussion started: 28 October 2019

doi:10.1007/s10347-009-0210-8, 2010.

Walsh, J. J., Watterson, J., Bailey, W. R. and Childs, C.: Fault relays , bends and branch-lines, , 21(8–9), 1019–1026, doi:10.1016/S0191-8141(99)00026-7, 1999.

Walsh, J. J., Bailey, W. R., Childs, C., Nicol, A. and Bonson, C. G.: Formation of segmented normal faults : a 3-D perspective, , 25, 1251–1262, doi:10.1016/S0191-8141(02)00161-X, 2003.

Wilkins, S. J., Naruk, S. J., Wilkins, S. J., International, S., Naruk, S. J. and International, S.: Quantitative analysis of slip-induced dilation with application to fault seal, , 1(1), 97–113, doi:10.1306/08010605177, 2007.

Woodcock, N. H., Dickson, J. A. D. and Tarasewicz, J. P. T.: Transient permeability and reseal hardening in fault zones : evidence from dilation breccia textures, Geol. Soc. London, Spec. Publ., 270, 43–53, 2007.

Wu, G., Gao, L., Zhang, Y., Ning, C. and Xie, E.: Fracture attributes in reservoir-scale carbonate fault damage zones and implications for damage zone width and growth in the deep subsurface, J. Struct. Geol., 118(February 2017), 181–193, doi:10.1016/j.jsg.2018.10.008, 2019.

Zhang, Y., Schaubs, P. M., Zhao, C., Ord, A., Hobbs, B. E. and Barnicoat, A. C.: Fault-related dilation, permeability enhancement, fluid flow and mineral precipitation patterns: numerical models, Geol. Soc. London, Spec. Publ., 299(1), 239–255, doi:10.1144/SP299.15, 2008.

Zhu, W. and Wong, T.-F.: The transition from brittle faulting to cataclastic flow: Permeability evolution, J. Geophys. Res., 102(96), 3027–3041, doi:10.1029/96JB03282, 1997.